INTERAGENCY REPORT: ASTROGEOLOGY 22

ESTIMATES OF THE MECHANICAL PROPERTIES OF LUNAR SURFACE USING TRACKS AND SECONDARY IMPACT CRATERS PRODUCED BY BLOCKS AND BOULDERS

By

H. J. Moore 1928–

July 1970

Prepared under NASA Contract no. R-66

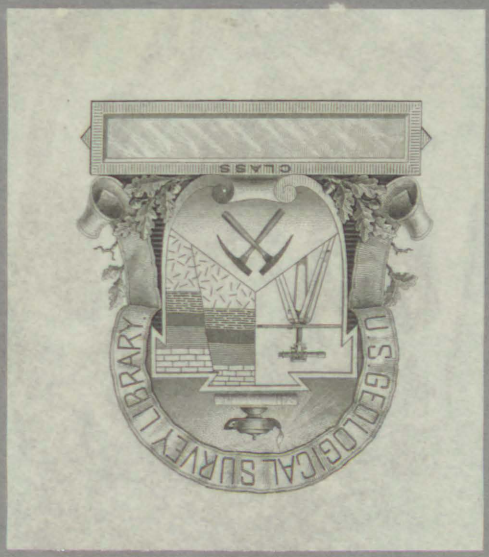

INTERAGENCY REPORT: ASTROGEOLOGY 22

ESTIMATES OF THE MECHANICAL PROPERTIES OF LUNAR SURFACE USING TRACKS AND SECONDARY IMPACT CRATERS PRODUCED BY BLOCKS AND BOULDERS

By

H. J. Moore 1928-

July 1970

Prepared under NASA Contract no. R-66

Weld - Int. 2905

[50)
[29s
[1486]

U.S. GEOLOGICAL SURVEY
WASHINGTON, D. C.
20242

[Open-file series]

For release OCTOBER 13, 1970

The U.S. Geological Survey is releasing in open file the following reports. Copies are available for inspection in the Geological Survey Libraries, 1033 GSA Bldg., Washington, D.C. 20242; Bldg. 25, Federal Center, Denver, Colo. 80225; and 345 Middlefield Rd., Menlo Park, Calif. 94025. Copies are also available for inspection in other offices as listed:

1. A gravity and aeromagnetic survey of the mid-Tertiary sedimentary basin on the south coast of Puerto Rico, by Andrew Griscom and William L. Rambo. 77 p., 42 figs. 504 Custom House, San Francisco, Calif. 94111; USGS, Lamar St. and Franklin Roosevelt Ave., San Juan, Puerto Rico 00963; Puerto Rico Econ. Development Admin., Dept. of Industrial Research, San Juan, Puerto Rico 00963. [Material from which copy can be made at private expense is available in the San Francisco office, and in the office of the Puerto Rico Econ. Development Admin., San Juan, P.R.]

2. Preliminary map of bedrock surface under parts of Boston, Cambridge, and Brookline, Massachusetts, by C. A. Kaye and others. 8 p., 1 map (scale 1:6,000). 80 Broad St., Boston, Mass. [Material from which copy can be made at private expense is available in the Boston office.]

3. Estimates of the mechanical properties of lunar surface using tracks and secondary impact craters produced by blocks and boulders, by H. J. Moore. 65 p., 11 figs., 7 tables. 601 E. Cedar Ave., Flagstaff, Ariz. 86001.

* * *

CONTENTS

ILLUSTRATIONS

TABLES

ESTIMATES OF THE MECHANICAL PROPERTIES OF LUNAR SURFACE USING TRACKS AND SECONDARY IMPACT CRATERS PRODUCED BY BLOCKS AND BOULDERS[1/]

by H. J. Moore

Abstract

Estimates of bearing capacities of lunar surfaces using tracks and secondary impact craters produced by blocks and boulders shown in photographs taken by Lunar Orbiters II and III are the same order of magnitude as those reported by the Surveyor project, but they are generally less.

Static analyses of 48 lunar blocks and boulders and their tracks yield friction angles between 10° and 30° and averaging about 17°. These values were computed using: (1) Terzaghi's bearing capacity equations for circular footings, (2) Meyerhof's dimensionless numbers for general shear on level surfaces, (3) a cohesion of 10^3 dynes per cm^2, (4) a density of 1.35 gm per cm^3 for the near surface materials, (5) a density of 2.7 gm per cm^3 for the block or boulder, (6) spheroidal (triaxial) boulders unless definite shapes can be established, (7) footing radii equal to the half-width of the block or boulder, the half-width of the track, and(or) the half-width of the shadow near the base of the block or boulder.

For 115 secondary impact craters and their corresponding blocks, dynamic strengths are estimated using: (1) the product of one-half the mass per unit area of the block and the normal component of velocity squared divided by the crater depth, and (2) the ratio of the kinetic energy of the block and the volume of the secondary crater. Velocities of the blocks are calculated using a ballistics equation and assuming an ejection angle of 45°. Block densities are taken as 2.7 gm per cm^3. Dynamic strengths of the near surface materials using the first procedure average 25.2×10^5 dynes per cm^2 (37 psi); and, for the second procedure, they average 19.2×10^5 dynes per cm^2 (28 psi). Comparison between dynamic strengths and expected static strengths, computed for each block using the assumptions above, show that most of the dynamic strengths correspond to the static strengths when the friction angle is 30° and larger.

Data on experimental low velocity impacts with natural targets are compared with the lunar data on secondary impacts. Nara's modified Poncelet equation for sand yields an average angle of internal friction near 34° using the appropriate block and soil constants mentioned above.

1/ Work performed on behalf of the National Aeronautics and Space Administration under contract number R-66.

Comparison of coefficients computed using the equations for sand of Clark and McCarty, Mortensen, and Moore for the lunar data with the corresponding constants for terrestrial data indicate the lunar coefficients are generally low. These low values can be brought into better agreement with terrestrial data on sand by increasing the assumed ejection angles to 60° or 70° and considering the effect of the low acceleration of gravity at the lunar surface.

Introduction

Five soft-landing Surveyor spacecraft have provided data on the mechanical properties of the lunar surface using touchdown dynamics, the lunar surface sampler, imprints of crushable blocks and other hardware, the reaction of lunar surface materials to vernier engine and rocket motor exhaust gases, and imprints made by small rolling stones set in motion by the spacecraft. As a result of these analyses, it was found that the materials at the lunar surface are very fine grained with mechanical properties somewhat like moist sand and that these materials have sufficient bearing capacity to support Apollo spacecraft and suitably designed vehicles.

Because the Surveyor program results represent five sample points covering an area of a few tens of square meters on a globe with an area of about 37×10^{12} square meters, additional information is sought for areas where Surveyors have not landed. Three methods of obtaining such data have been proposed:

1. Slope stability analyses (Choate, 1966; Jaffe, 1965),
2. Analyses of boulders[1/] and their corresponding tracks (Eggleston and others, 1968; Felice, 1967),

---

1/ Boulders are conventionally defined as rounded rocks with diameters larger than 256 mm. For convenience here, the term boulder will be used to describe large rocks, either angular or rounded, at the end of long tracks.

3. Secondary impact craters around small lunar craters and their corresponding blocks[1/] (see for example Kuiper and others, 1966, p. 153).

Some 300 or more tracks produced by moving boulders (rounded and angular) have been identified on photographs taken by Lunar Orbiters (Grolier and others, 1968). The tracks represent failure and deformation of the lunar surface material by a boulder as it moved downslope (fig. 1). Thus, the surface materials have failed and the boulder at the end of the track is demonstrably resting on the lunar surface. Sizes of boulders associated with tracks range from about 1 m across to about 50 m across. The smallest tracks produced are those made when Surveyors III and V set centimeter size rocks in motion (see for example, Shoemaker and others, 1967, p. 26, fig. 3-17a). The morphologies of the tracks shown on Orbiter photographs indicate several kinds of boulder motion: (1) periodic elliptical depressions suggest bouncing, (2) short uniform tracks suggest skidding, (3) long uniform tracks suggest rolling, and (4) continuous tracks with deep depressions that alternate from side to side suggest "walking".

Analysis of the dynamic aspects of the tracks appears to be a formidable task at this time; however, the manner in which boulders at the end of tracks might be used to estimate static bearing capacities has been illustrated by several authors (Eggleston and others, 1968; Felice, 1967; Shoemaker and others, 1967).

Secondary impact craters are found around some fresh craters such as those shown in Lunar Orbiter II and III photographs

---

[1/] Blocks are angular rocks with diameters larger than 256 mm. For convenience here, the term block will be used to describe large rocks associated with secondary impact craters.

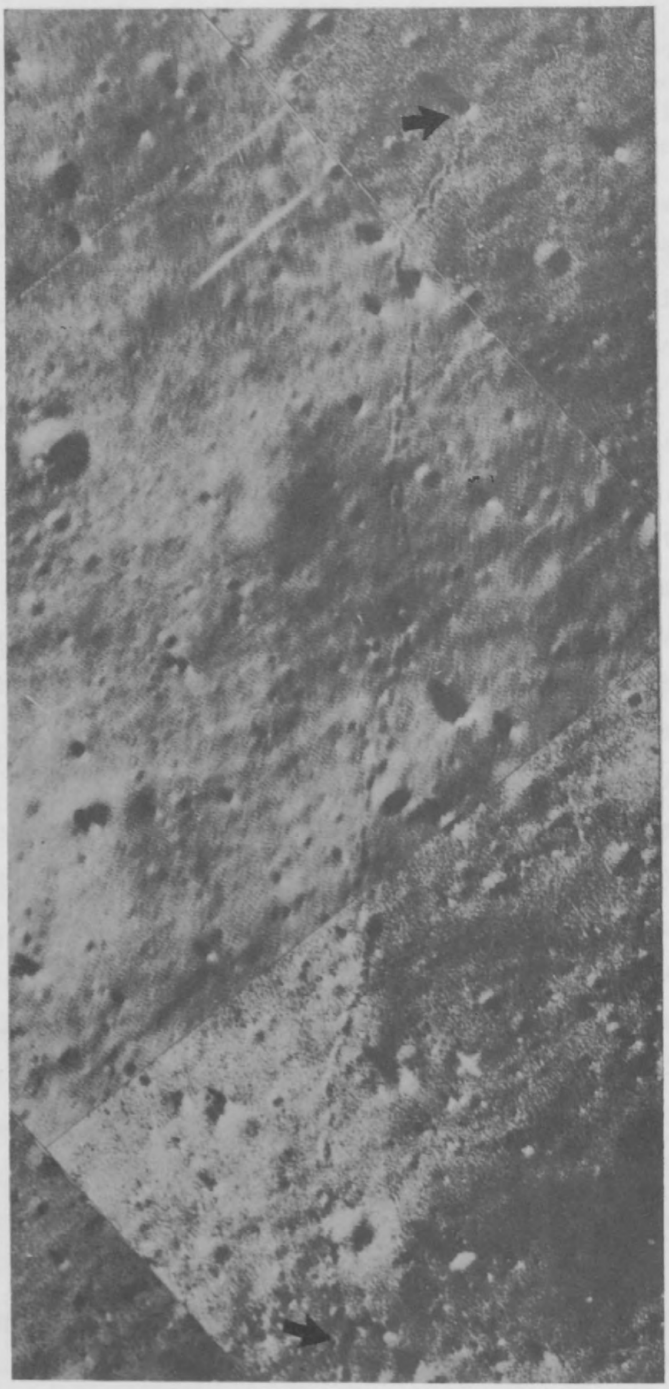

Figure 1.--Boulder track with periodic elliptical depressions in crater Sabine EA in Mare Tranquillitatis. Boulder is 2.8x2.8x 2.8 m. Upper arrow shows boulder; lower arrow shows part of track. This boulder is the same as Boulder D of Eggleston and others (1968, fig. 15, p. 254). (Photograph is Lunar Orbiter II high-resolution frame H71.)

Figure 2.--Crater with blocky ejecta and secondary impact craters 50 km north of Flamsteed in Oceanus Procellarum. Crater is about 500 m across. Arrows show two secondary impact craters and the blocks that produced them. (Photograph is Lunar Orbiter III high-resolution frame H189.)

(Moore and Lawry, 1968). Many of these secondary craters, which are produced by the impact of blocks and debris ejected from a larger nearby parent crater, may be recognized by their morphology and distribution around the parent crater. Examples of such secondary craters and their parent crater are shown in figure 2. The parent crater has a sharp, well-defined rim lined with large blocks. Crater walls and internal terraces are also sharp and littered with blocks. A continuous blocky-ejecta blanket surrounds the crater. Secondary impact craters and scattered blocks deposited discontinuously along radial lines occur from several tens of meters to at least 500 m from the crater rim. In a few places, elongate secondary craters alined along radials from the parent crater have blocks near their distal tips (see fig. 2); crater diameters are comparable to the dimensions of the associated block. Thus, in some cases, it is possible to assign a given block with a given secondary crater and then assign both with their parent with confidence.

When the proper association of block, secondary crater, and parent crater are made, an estimate of the dynamic penetration resistance could be made if sufficient information were available such as block density, block shape, block velocity at impact, block rotational velocity, angle of impact, and crater dimensions. Much of the necessary information must be assumed and some of it estimated. To date, only preliminary attempts to utilize secondary impact craters to estimate bearing capacities have been made (Moore, 1967a, 1967b).

This report summarizes results using methods 2 and 3 (p. 2-3) for 48 boulders at the end of tracks and 115 secondary impact craters shown in photographs taken by Lunar Orbiters II and III.

Measurements and procedures

The boulder tracks and craters with secondary impact craters were located by visually scanning Lunar Orbiter high-resolution photographs; and, when found, they were located on standard Lunar Orbiter prints (≈ 7.2x enlargements of the spacecraft film) by mission number, frame number, framelet number, and distance from the data edge. Table 1 contains a list of these features on Lunar Orbiter II and III photographs.

Working prints of the Lunar Orbiter photographs containing the tracks and secondary craters were obtained by enlarging first generation negatives five times. This represents an enlargement of 36 times the image size on the spacecraft film. Several enlargements were less (≈ 14x enlargements of the spacecraft film). Enlargements of working prints were computed in two ways which always agreed within a few percent: (1) by computation of the enlargement of the standard print using the framelet length on the spacecraft (5.5 cm) and then the enlargement factor of the working print by comparison of distances of corresponding marks on the standard prints and the working prints, and (2) by computation of enlargement of the working print using the framelet width on the spacecraft film (0.254 cm). Scales of the spacecraft film were obtained from data books (Boeing Company, 1967a, 1967b) and then combined with the enlargements to give the scale of the standard and working prints. Tilt effects were assessed using the magnitudes to the frame corners listed in the data books. When tilt effects on scales at the corners of the frame were less than 5 percent of the scale at the center, they were ignored. Sun angles and directions used in conjunction with shadow lengths, were obtained from the data books.

Boulder, track, and crater dimensions were measured on the working prints and the images of both the working prints and standard prints were simultaneously examined and occasionally, as a check, both were measured. Crater diameters and track widths were measured from rim to rim and depths were estimated

Table 1.--Data on secondary impact craters and boulder tracks seen on Lunar Orbiter II and III photographs

The meanings of the headings in table 1 are as follows:

A. Location: description of location of features used on Lunar Orbiter II and III photographs and on the moon

1. Site
   a. Arabic number pertains to feature number. This number corresponds to the numbers in column 1 on table 2.
   b. Roman numeral designates mission number, i.e., Lunar Orbiter II or Lunar Orbiter III.
   c. P, plus number-letter designations indicate Lunar Orbiter site designations.
2. Frame
   a. H refers to high-resolution photograph.
   b. Number refers to frame number.
3. Framelet
   a. Number refers to number of framelet strip on data edge of individual frame.
4. Distance
   a. The distance from the data edge (in centimeters) on a standard Lunar Orbiter print ($\approx$ 7.2 enlargement of the spacecraft film) to the boulder at the end of a track or to a parent crater surrounded by secondary impact craters.
5. Lat. Long.

   The approximate selenographic coordinates of the boulder track or secondary impact craters.

B. Crater: dimensions of a secondary crater

1. Width

   Width of secondary crater in meters calculated from photographic measurements and appropriate scales.
2. Length

   Length of secondary crater in meters calculated from photographic measurements and appropriate scales.
3. Depth

   Depth of secondary crater in meters calculated from photographic measurements of shadow length, the tangent of the sun angle, and appropriate scales.

4. Volume

Volume of secondary impact crater in units of $10^6 cm^3$ (or cubic meters) using dimensions in 1, 2, and 3 above and assuming a triaxial hemispheroidal crater.

C. Block: dimension of block that produced corresponding secondary impact crater or boulder at end of track.

1. Width

Width of block in meters calculated from photographic measurements and appropriate scales.

2. Length

Length of block or boulder in meters calculated from photographic measurements and appropriate scales.

3. Height

Height of block or boulder in meters calculated from photographic measurements of length of shadows, the tangent of the sun angle, and appropriate scales. Where interpretation warrants, depth of track near boulder or block is added.

4. Mass

Mass of block or boulder in units of 10^6 gms (or metric tons) computed from dimensions in 1, 2, and 3 and assuming a triaxial spheroidal shape unless definite shapes could be established. When shapes could be established the shape is designated by a superscript lower case letter as follows: s - spherical, hs hemispherical, r - rectangular.

D. Track: dimensions of track

1. Width

Width of track in meters near block or boulder analyzed with the static bearing capacity equation (equation 2).

2. Length

Length of track in meters near block or boulder. Commonly but not always used with 1 above to calculate bearing area.

3. Depth

Depth of track near block or boulder in meters calculated from photographic measurements of shadow lengths, the tangent of the sun angle, and appropriate scales. This value is used for footing depth in equation 2.

4. Area

Area used in bearing pressure calculations in conjunction with equation 2, and best estimate of the bearing area using minimum value of track width, or boulder width at base of boulder. In general, bearing area is assumed elliptical or spherical.

Table 1.--Data on secondary impact craters and boulder

	Site	Frame	Location Framelet	Distance (cm)	Lat. (degrees)	Long. (degrees)	Crater Width (m)	Length (m)	Depth (m)	Volume ($10^6 cm^3$)
1.	IIP 1	H19	861	27.3	4.1	37.8	1.7	4.7	0.96	4.0
2.	IIP 1	H20	991	21.1	4.1	38.0				
							1.3	4.3	0.14	0.40
3.	IIS 2A	H27	921	21.2	3.8	36.6				
4.	IIP 2	H41	775	35.0	2.7	34.4	4.9	6.5	0.93	16.0
							3.0	9.7	0.51	7.7
5.	IIP 3A	H48	708	21.7	4.4	21.5	8.1	9.4	0.51	20.0
							2.1	4.8	0.32	1.7
6.	IIP 3A	H50	932	10.6	4.6	21.8				
7.	IIP 3B	H55	597	8.1	4.3	21.1				
							2.6	5.0	0.34	2.3
8.	IIP 4	H65	986	9.5	4.5	15.8				
9.	IIP 5	H71	710-713	20.8	2.8	2.5				
10.	IIP 6A	H76	364	13.0	1.3	23.7				
11.	IIP 7B	H106	292	9.5	2.2	2.1				
12.	IIP 8	H123	595	2.6	$\bar{1}$.3	0.0				
13.	IIP 10A	H149	924	5.6	3.8	$\bar{2}$7.2				
14.	IIP 10A	H150	081	13.1	3.8	$\bar{2}$7.1				
							5.5	8.1	0.23	5.3
15.	IIP 10B	H154	641	3.3	3.2	$\bar{1}$3.7	4.8	7.2	0.59	11.0
							4.3	6.0	0.35	4.7
							3.6	4.6	0.43	3.7
16.	IIP 10B	H159	315	38.9	2.9	$\bar{2}$6.9				
17.	IIP 10B	H160	386	26.4	3.2	$\bar{2}$6.8				
							2.6	5.9	0.29	2.3
18.	IIP 11A	H163	783	25.1	0.3	$\bar{2}$0.2				
19.	IIP 11A	H164	915	9.5	0.3	$\bar{2}$0.1	3.0	33.0	0.84	43.0
							3.6	22.2	1.0	41.0
20.	IIP 11A	H165	016	20.7	0.4	$\bar{2}$0.1	4.2	9.6	0.81	17.0
21.	IIP 11A	H166	150	13.8	$\bar{0}$.4	$\bar{1}$9.7	3.8	8.9	1.2	21.0
22.	IIP 11B	H177	436	33.0	$\bar{0}$.4	$\bar{1}$9.2	6.6	8.0	2.1	59.0
							8.3	9.9	2.3	98.0
							5.5	6.6	2.0	37.0
							6.1	7.2	1.6	37.0
							9.3	11.5	2.6	142.0
							6.6	11.0	2.0	75.0
23.	IIP 12A	H179	847	19.5	2.6	$\bar{3}$4.5	4.0	5.5	0.24	2.8
							4.0	2.6	0.50	2.7
							2.6	2.6	0.38	2.7
							2.4	7.6	0.30	2.8

tracks seen on Lunar Orbiter II and III photographs[1/]

Block				Track			
Width (m)	Length (m)	Height (m)	Mass (10^6 grams)	Width (m)	Length (m)	Depth (m)	Area (m^2)
1.7	2.1	1.4	7.0				
2.1	2.1	1.5	9.3	1.9	2.1	shallow	3.3
1.3	1.3	0.54	1.3				
6.0	6.0	3.1	305.0[s]	6.0	21.4	0.6	28.0
2.4	1.8	2.1	13.0				
2.6	2.6	1.4	13.0				
5.6	6.7	2.0	105.0				
3.2	3.2	1.4	20.0				
2.9	2.9	2.9	36.0[hs]	2.9	2.9	0.27	6.7
2.1	1.6	1.0	9.0[r]	1.6	2.1	shallow	3.4
2.4	2.4	1.2	10.0				
6.7	6.7	6.2	393.0	6.7	11.0	0.44	35.0
2.8	2.8	2.8	31.0	1.3	1.3	0.26	1.3
8.5	8.5	7.7	786.0	5.1	5.1	0.46	19.5
2.45	3.0	1.5	16.0	0.95	2.1	0.17	1.6
5.2	5.2	5.2	196.0[s]	1.7	1.7	1.0	9.1
4.0	5.0	1.7	50.0	2.4	4.0	0.26	7.7
2.4	2.4	1.6	13.0	1.8	1.8	n.m.	2.5
3.4	3.6	1.3	22.0				
3.1	3.1	1.2	16.0				
3.1	3.1	0.7	9.4				
1.9	1.9	1.0	5.1				
2.8	3.2	3.0	38.0	2.8	3.2	0.10	7.0
1.8	2.8	1.2	8.5	1.9	1.8	0.10	2.7
1.8	1.8	1.8	8.2				
5.4	5.4	3.3	132.0	4.0	5.4	1.0	17.0
3.0	3.6	2.2	33.0				
2.6	3.0	1.7	18.0				
2.4	2.4	1.7	13.0	2.4	2.4	n.m.	4.5
3.0	3.6	2.1	32.0				
2.4	2.4	2.3	18.0-34.0	1.6	3.0	0.40	3.8
3.3	3.8	3.6	64.0				
4.4	4.4	3.6	99.0				
3.8	7.8	3.6	153.0				
6.1	9.4	6.1	490.0				
3.3	3.3	3.2	49.0				
3.3	3.3	2.2	34.0				
2.4	2.4	2.4	19.0[s]				
1.8	1.8	1.5	6.8				
2.0	1.8	1.4	7.1	1.4	1.4	small	1.5
2.0	2.2	1.1	6.8				
3.0	3.0	1.5	19.0				

Table 1.--Data on secondary impact craters and boulder

	Site	Frame	Location Framelet	Dist-ance	Lat.	Long.	Crater Width	Length	Depth	Volume
				(cm)	(degrees)		(m)	(m)	(m)	($10^6 cm^3$)
24.	IIP 12A	H179	884	38.9	2.4	$\overline{3}4.5$				
25.	IIP 12A	H179	917	25.7	2.3	$\overline{3}5.5$	3.0	4.5	0.40	2.8
							3.3	3.5	0.35	2.1
							4.6	6.3	0.63	8.9
							4.5	5.0	0.70	8.2
							4.0	6.3	0.48	6.3
							4.3	5.0	0.63	7.0
26.	IIP 12A	H186	779	34.5	2.4	$\overline{3}3.6$	5.7	12.7	1.1	41.0
							3.1	5.7	1.0	9.0
27.	IIP 12A	H187	925	16.3	2.1	$\overline{3}4.5$	5.4	7.6	0.88	18.8
							5.1	6.1	0.80	13.0
							2.6	7.6	0.53	5.4
28.	IIP 12B	H189	166	6.3	2.1	$\overline{3}4.2$	3.1	4.4	0.37	2.6
							3.4	5.8	0.61	6.3
							2.4	5.8	0.48	3.5
29.	IIP 12B	H190	323	2.8	2.0	$\overline{3}4.1$	2.5	3.3	0.43	1.8
30.	IIP 12B	H192	596	26.4	1.8	$\overline{3}3.8$	1.7	2.8	0.45	1.1
							3.0	4.7	0.43	3.2
31.	IIP 12B	H193	723	30.4	1.8	$\overline{3}3.7$	2.5	4.5	0.29	1.7
							2.9	4.1	0.29	1.8
							4.9	8.2	0.88	18.4
32.	IIP 13A	H195	975	19.2	2.9	$\overline{4}2.7$	3.7	3.7	0.64	4.6
							4.7	8.4	0.74	15.2
							2.7	3.7	0.27	1.4
							3.3	5.8	0.31	3.1
33.	IIP 13A	H198	397	39.1	1.9	$\overline{4}2.0$				
34.	IIP 13B	H210	954	22.1	1.5	$\overline{4}1.5$	2.3	3.2	0.49	2.9
							2.3	3.0	0.40	1.4
							2.3	2.8	0.49	1.6
							2.3	3.0	0.40	1.4
							3.8	4.0	0.49	3.9
							4.7	5.5	0.57	7.7
							4.2	5.3	0.89	10.0
35.	IIP 13B	H211	049	26.5	1.6	$\overline{4}1.3$				
36.	IIIP-2	H26	293-295	2.9	$\overline{0}.4$	42.1				
37.	IIIP-2	H35	395-396	25.8	$\overline{0}.7$	42.9				
38.	IIIP-5	H52	676-679	20.5	0.4	24.1	2.3	7.0	0.21	1.8
39.	IIIP-6	H68	732-734	20.5	0.9	$\overline{0}.9$	4.5	4.5	0.49	5.2
40.	IIIP-7	H100	941-943	19.0	0.9	$\overline{0}.9$	1.9	2.8	0.30	0.83
							3.2	3.2	0.40	2.1
							1.5	1.5	0.20	0.23

tracks seen on Lunar Orbiter II and III photographs[1/]

Block				Track			
Width	Length	Height	Mass	Width	Length	Depth	Area
(m)	(m)	(m)	(10^6 grams)	(m)	(m)	(m)	(m^2)
2.2	2.8	1.3	11.0	1.0	2.0	0.18	1.6
1.3	1.8	0.63	2.1				
1.5	1.8	0.93	3.5				
3.3	3.5	1.6	26.0				
2.3	2.3	0.70	5.2				
3.8	3.8	2.0	40.0				
2.5	2.8	0.86	8.4				
3.1	3.4	2.6	38.0				
1.8	1.6	0.88	3.6				
2.8	2.8	1.8	20.0				
1.5	1.5	0.8	2.6				
2.5	2.6	1.9	18.0				
1.4	1.7	0.61	2.0				
1.4	1.7	1.2	4.0				
1.7	2.0	0.85	4.0				
2.0	2.0	2.2	13.0	1.0	1.0	0.14	0.78
2.0	2.5	1.4	9.6	1.2	1.2	shallow	1.1
2.0	2.2	1.1	6.8				
2.4	3.7	1.3	16.0				
2.5	2.5	1.2	11.0				
2.5	3.3	2.3	27.0				
2.5	3.3	1.6	18.0				
2.1	2.3	0.84	5.7				
3.3	3.9	1.9	34.0				
1.4	1.4	0.51	1.4	0.40	1.4	0.05	0.56
2.1	2.3	0.62	4.2				
4.9	5.7	2.4	94.0	3.1	5.7	0.49	14.0
2.3	2.8	1.3	12.0				
1.9	1.9	0.81	4.1				
2.5	2.8	1.5	15.0				
1.3	1.5	0.64	1.7				
2.1	2.3	1.3	8.8				
1.5	3.4	2.1	15.0				
2.3	2.8	1.3	12.0				
3.8	4.6	3.3	157.0	1.8	2.4[r]	1.0	4.3[r]
8.8	8.8	5.7	624.0	4.8	4.8	0.62	18.0
4.1	4.4	4.5	113.0	2.8	2.8	0.69	6.2
1.7	1.9	1.5	6.8	1.4	1.4	0.21	1.5
2.0	4.0	2.0	22.4	1.8	2.0	0.22	2.8
1.7	2.1	0.8	4.0				
1.3	1.3	0.5	1.2				
1.1	1.1	0.4	6.8				

Table 1.--Data on secondary impact craters and boulder

Site	Frame	Location				Crater			
		Framelet	Distance	Lat.	Long.	Width	Length	Depth	Volume
			(cm)	(degrees)		(m)	(m)	(m)	(10^6 cm^3)
41. IIIP-7	H100	910	10.4	0.9	$\overline{1}$.0				
42. IIIS-16	H107	868-871	2.1	0.7	$\overline{0}$.9				
43. IIIS-17	H111	373	38.9	$\overline{4}$.9	4.9				
44. IIIS-19	H118	305-307	31.2	$\overline{3}$.4	$\overline{3}$.4				
45. IIIP-8	H125	206	8.7	0.6	20.1				
46. IIIP-8	H130	895-898	9.6	$\overline{0}$.9	$\overline{19}$.5				
						2.0	2.0	0.20	1.7
47. IIIP-9B	H146	935	2.7	$\overline{2}$.4	$\overline{23}$.0	2.0	4.3	0.43	1.9
						2.4	4.8	0.43	2.6
48. IIIP-9B	H149	408-409	28.3	$\overline{3}$.0	$\overline{22}$.7				
49. IIIP-9B	H151	678	33.7	$\overline{3}$.2	$\overline{22}$.5	8.7	20.7	1.3	122.0
						4.4	5.7	0.44	5.7
						3.9	6.6	0.52	7.0
50. IIIP-9C	H158	541-543	39.2	$\overline{3}$.1	$\overline{22}$.8				
51. IIIP-9C	H159	674	3.1	$\overline{3}$.1	$\overline{22}$.9				
52. IIIP-10	H164	340-346	7.5	1.8	$\overline{42}$.4	3.0	4.7	0.37	2.7
						5.7	10.0	0.70	21.0
						7.5	12.4	1.4	68.0
						7.0	6.0	1.1	24.0
						7.5	7.5	1.4	41.0
						6.2	6.2	1.3	26.0
						4.5	5.5	1.1	14.0
						3.0	4.2	1.4	9.0
53. IIIP-10	H164	379-380	1.7	1.5	$\overline{42}$.5	2.5	14.4	0.80	15.0
54. IIIP-10	H170	126-128	10.3	1.4	$\overline{41}$.5	7.4	7.4	0.76	22.0
						4.7	8.6	1.2	25.0
						4.7	5.4	0.76	10.0
55. IIIP-12B	H181	563-568	28.5	$\overline{2}$.1	$\overline{43}$.5	3.2	3.2	0.44	2.3
						4.9	7.3	0.73	14.0
						2.9	8.6	0.37	4.8
						7.3	12.2	1.1	51.0
						4.9	5.4	0.73	11.0
						3.7	5.9	0.59	6.7
56. IIIP-12A	H186	231	8.2	$\overline{2}$.2	$\overline{44}$.6	3.1	4.8	0.38	2.9
57. IIIP-12A	H186	193	28.4	$\overline{2}$.1	$\overline{44}$.5				
58. IIIP-12A	H188	527-531	8.4	$\overline{2}$.5	$\overline{44}$.4	6.0	12.0	0.76	28.0
59. IIIP-12A	H189	664-667	26.5	$\overline{2}$.7	$\overline{44}$.3	3.8	4.3	0.53	4.5
						3.4	4.8	0.53	4.5

tracks seen on Lunar Orbiter II and III photographs

Block				Track			
Width	Length	Height	Mass	Width	Length	Depth	Area
(m)	(m)	(m)	(10^6 grams)	(m)	(m)	(m)	(m^2)
4.7	4.7	2.4	74.0	4.7?	4.7?	?	17.0
2.6	3.0	3.0	32.0[r]	0.8	2.6	0.4	2.1[r]
2.6	4.0	2.2	32.0	2.6	4.0	?	≈6.3
5.1	5.2	4.9	184.0	4.1	4.1	<0.9	13.0
2.4	2.6	2.4	18.0	2.2	2.2	0.50	3.8
2.45	2.45	2.45[s]	21.0	1.8	1.8	0.12	2.7
1.4	2.6	1.2	51.0	1.2	1.2	0.24	1.1
1.6	3.1	1.2	8.4	1.2	1.2	0.12	1.1
4.1	4.1	4.1	96.0	2.9	2.9	0.43	6.4
1.8	1.8	1.1	5.0	1.2	1.4	0.12	1.3
2.0	2.9	1.6	1.2	1.6	1.6	0.12	2.0
1.6	1.8	1.6	6.5	1.2	1.2	0.12	1.1
2.0	2.6	1.9	14.0	1.7	1.7	0.43	2.3
2.6	2.6	0.87	8.2	1.1	1.1	0.43	0.95
5.0	5.0	5.0	117.0	3.3	3.3	0.88	8.6
7.6	7.6	3.7	299.0				
3.1	3.1	1.6	22.0				
3.1	3.1	2.4	32.0				
2.9	2.9	2.9[s]	34.0[s]	2.5	2.5	0.45	4.9
3.2	3.2	2.0	29.0	2.2	2.3	0.29	4.0
2.0	2.0	1.1	6.2				
2.2	2.5	1.1	8.5				
4.2	4.7	2.4	66.0				
1.7	2.5	0.95	5.6				
3.0	3.2	0.85	11.0				
2.5	3.0	0.95	10.0				
1.7	3.0	1.2	8.6				
1.7	2.0	1.0	4.8				
4.0	6.2	0.95	33.0				
2.9	2.4	1.8	18.0				
2.0	2.7	2.1	16.0				
2.2	2.4	1.3	9.6				
2.2	2.4	1.4	10.0				
2.4	2.7	1.5	14.0				
4.4	4.4	2.2	60.0				
5.6	5.6	1.8	79.0				
2.2	2.4	1.0	7.4				
2.0	2.4	1.5	10.0				
3.3	3.8	1.3	23.0	2.4	3.1	0.38	5.8
4.1	4.5	2.9	74.9	2.4	2.4	0.37	0.78
2.9	5.2	1.5	32.0				
1.4	1.7	1.2	4.0				
1.7	2.4	1.1	6.3				

Table 1.--Data on secondary impact craters and boulder

Site	Frame	Location: Framelet	Location: Distance (cm)	Location: Lat. (degrees)	Location: Long. (degrees)	Crater: Width (m)	Crater: Length (m)	Crater: Depth (m)	Crater: Volume ($10^6 cm^3$)
60. IIIP-12A	H189	621	8.0	$\overline{2}.4$	$\overline{4}4.2$	7.8	9.6	1.9	74.0
						13.2	19.2	2.3	303.0
						12.0	24.0	2.9	434.0
						11.0	19.2	2.3	253.0
						21.0	39.0	3.8	1618.0
61. IIIP-12A	H192	007-009	28.1	$\overline{2}.5$	$\overline{4}3.7$	2.6	4.3	0.55	3.2
						4.8	6.5	0.62	10.0
						4.8	6.0	0.79	1.2
62. IIIP-12A	H194	282-288	15.0	$\overline{2}.8$	$\overline{4}3.6$	8.2	9.6	1.2	49.0
						4.1	7.2	0.72	11.0
						5.3	7.4	0.82	17.0
						5.3	7.2	0.72	14.0
						5.5	5.5	0.65	10.0
						4.6	5.8	0.82	11.0
						6.0	6.0	0.96	18.0
						1.9	3.1	0.27	12.0
						2.4	12.0	0.64	9.6
63. IIIP-12A	H197	666-668	1.0	$\overline{2}.8$	$\overline{4}3.1$	3.4	4.1	0.41	3.0
						2.6	2.6	0.41	1.4
64. IIIP-12A	H199	925-926	18.1	$\overline{2}.9$	$\overline{4}2.7$	2.3	3.5	0.49	2.1
						2.6	6.3	0.42	3.6
						2.8	4.9	0.42	3.0
65. IIIP-12A	H200	101-103	6.4	$\overline{3}.2$	$\overline{4}2.8$				
66. IIIP-12b.1	H204	601-602	11.5	$\overline{3}.1$	$\overline{4}3.1$	3.6	5.3	0.73	7.2
67. IIIP-12b.1	H204	566-567	11.2	$\overline{2}.9$	$\overline{4}3.1$	2.9	3.6	1.3	7.1
						3.4	5.1	0.63	5.7

tracks seen on Lunar Orbiter II and III photographs

Block				Track			
Width	Length	Height	Mass	Width	Length	Depth	Area
(m)	(m)	(m)	(10^6 grams)	(m)	(m)	(m)	(m^2)
5.4	9.0	4.6	313.0				
4.8	7.8	8.4	440.0				
17.0	20.0	6.6	3140.0				
10.0	11.4	3.6	575.0				
10.0	16.0	11.0	2464.0				
1.7	1.9	0.79	3.6				
2.4	2.4	0.96	7.7				
2.4	3.6	0.96	12.0				
3.6	4.1	1.4	29.0				
2.9	2.9	1.1	13.0				
2.6	4.3	1.4	22.0				
2.9	3.1	2.0	25.0				
2.4	2.6	1.1	9.6				
2.9	2.9	0.82	9.6				
3.1	3.1	1.5	20.0				
0.90	0.90	0.40	6.5				
3.4	4.1	1.2	23.0				
1.4	1.0	0.50	0.98				
1.4	1.7	0.74	2.5				
0.93	1.4	0.49	0.89				
1.9	2.1	0.88	4.9				
0.93	1.2	0.81	1.3				
3.5[r]	4.0	3.3	125.0[r]	3.0	3.5	0.49	11.0[r]
2.2	2.4	1.4	10.0	1.7	2.4	0.73	3.2
1.7	1.7	0.92	3.7				
1.7	1.7	1.4	5.7				

Table 2.--Calculations of velocities, strengths, and constants from data in table 1.

The meanings of the headings in table 2 are as follows:

Column 1. Number corresponds to first arabic number under Location-Site in table 1.

Column 2. Velocity of block ejected from primary crater calculated using distance (or range) to secondary, and equation 1.

Column 3. Penetration resistance in units of 10^5 dynes per cm^2 (or newtons per cm^2) using the Euler equation (equation 3).

Column 4. Penetration resistance in units of 10^5 dynes per cm^2 (or newtons per cm^2) using twice the Charters-Summers equation (equation 4).

Column 5. The bearing pressure of a boulder on lunar surface computed as the product of the mass per unit area (boulder or block mass divided by track area) and the acceleration of gravity at the lunar surface in units of 10^5 dynes per cm^2 (or newtons per cm^2).

Column 6. The angle of internal friction computed using bearing pressure numbers in column 5 and equation 2. Friction angles were calculated only for boulders where bearing areas could be approximately assessed.

Column 7. The bearing capacity computed using equation 2 for blocks producing secondary impact craters assuming a friction angle of 35° and a cohesion of 10^3 dynes per cm^2. Block dimensions were used for footing size and depth of corresponding secondary crater were used for footing depth.

Column 8. Ratio of values in columns 3 and 7.

Column 9. Ratio of values in column 4 and 7.

Column 10. Estimates of friction angle for secondary impact craters using the Nara equation (equation 6), appropriate block and crater dimensions and assumptions mentioned in text.

Column 11. Coefficients for secondary impact craters (M) calculated using the Mortensen equation (equation 8).

Column 12. Coefficients (J/2) for secondary impact craters using the Clark and McCarty equation (equation 10).

Column 13. Coefficients (γ) for secondary impact craters using the Sandia empirical equation (equation 11).

Column 14. Coefficients ($\sqrt{\rho g' H/2}$) calculated for secondary impact craters using the Moore equation (equation 12).

Column 15. Coefficients (T) calculated for secondary impact craters using equation 13.

Table 2.--Calculations of velocities, strengths,

1	2	3	4	5	6	7	8
	Velocity	S_E (equation 3)	$2S_c$ (equation 2)	B	Φ_B (equation 2)	Q_{35} (equation 2)	$\frac{S_E}{Q_{35}}$
	m per sec	10^5 dynes per cm^2	10^5 dynes per cm^2	10^5 dynes per cm^2	degrees	10^5 dynes per cm^2	
1.	6.7	3.0	2.8	0.4		15	0.20
2.				0.5	10-15		
	10.2	18.0	11.0	0.2		6.2	2.9
3.				1.8	15		
4.	21.0	43.0	13.0	0.6		16	2.7
	9.1	10.0	5.0	0.4		14	0.71
5.	11.0	20.0	20.0	0.6		25	0.80
	13.0	34.0	74.0	0.4		14	2.4
6.				0.9	15		
7.				0.3	10-15		
	10.5	18.0	17.0	0.4		12	1.5
8.				1.8	15		
9.				3.8	30		
10.				6.5	25-30		
11.				1.6	20		
12.				3.5	20		
13.				1.1	10-15		
14.				0.9	15-20		
	10.0	26.0	15.0	0.4		14	1.9
15.	10.4	10.0	6.0	0.4		16	0.62
	11.5	12.0	9.4	0.2		14	0.86
	19.5	40.0	18.0	0.3		11	3.6
16.				0.8	15-20		
17.				0.5	15		
	9.0	22.0	10.0	0.5		9.2	2.4
18.				1.3	10		
19.	14.8	25.0	5.8	0.6		19	1.3
	14.0	15.0	3.0	0.5		19	0.79
				0.5	15		
20.	9.1	9.6	5.6	0.6		18	0.53
21.	12.0	13.0	4.4	0.7-1.5	15-20	19	0.68
22.	39.0	110.0	58.0	1.0		31	3.5
	28.0	54.0	28.0	1.1		35	1.5
	24.0	46.0	82.0	1.1		36	1.3
	18.0	54.0	150.0	1.8		40	1.4
	31.0	54.0	12.0	0.9		34	1.6
	32.0	52.0	17.0	0.6		29	1.8
23.	18.4	150.0	84.0	0.7		11	14
	15.6	32.0	22.0	0.4		11	3.3
				0.8	20-25		
	9.6	12.0	16.0	0.3		11	1.1
	7.2	12.0	12.0	0.4		13	0.92
24.				1.2	15-20		

and constants from data in table 1.

9	10	11	12	13	14	15
$\frac{2S_c}{Q_{35}}$	Φ (equation 6) degrees	M (equation 8) cgs units	J/2 (equation 10) cgs units	γ (equation 11) cgs units	$\sqrt{\rho g' H/2}$ (equation 12) cgs units	T (equation 13) cgs units
0.19	15-20	8	5.1	0.0016	39	99
0.92	≈ 40	83	30	0.015	260	350
0.79	30-35	10	13	0.019	150	320
0.35	30-35	11	11	0.005	93	210
0.80	30-35	27	15	0.009	140	350
5.3	35-40	72	25	0.018	230	480
1.4	35-40	38	18	0.010	160	330
1.1	35-40	33	33	0.014	240	620
0.38	30-35	14	11	0.006	95	190
0.67	30-35	35	15	0.009	130	200
1.7	40-45	31	20	0.024	220	330
1.1	≈ 40	18	22	0.011	190	490
0.31	35-40	6	12	0.011	120	300
0.16	30-35	4	8.9	0.007	87	190
0.31	25-30	8	9.4	0.004	78	220
0.23	30-35	5	8.0	0.005	74	200
1.9	40-45	16	12	0.034	160	370
0.80	35-40	10	8.8	0.017	110	280
2.3	30-35	33	9.1	0.015	110	290
3.8	35-40	45	12	0.014	130	490
0.35	30-35	4	8.3	0.017	110	250
0.59	35-40	9	9.2	0.020	120	230
7.6	> 45	63	52	0.061	560	1300
2.0	≈ 40	30	17	0.017	180	350
1.5	30-35	45	15	0.007	130	250
0.92	30-35	31	19	0.006	150	370

Table 2.--Calculations of velocities, strengths,

1	2	3	4	5	6	7	8
	Velocity	S_E (equation 3)	$2S_c$ (equation 2)	B	δ_β (equation 2)	Q_{35} (equation 2)	$\frac{S_E}{Q_{35}}$
	m per sec	10^5 dynes per cm^2	10^5 dynes per cm^2	10^5 dynes per cm^2	degrees	10^5 dynes per cm^2	
25.	13.6	13.0	5.0	0.2		9.2	1.7
	14.0	23.0	12.0	0.3		9.2	2.5
	9.1	9.3	8.4	0.5		17	0.55
	13.0	7.1	3.6	0.2		18	0.39
	8.8	14.0	18.0	0.6		17	0.82
	16.0	16.0	11.0	0.3		15	1.1
26.	18.0	35.0	11.0	0.8		21	1.7
	16.0	11.0	3.8	0.3		15	0.73
27.	19.0	32.0	13.0	0.5		18	1.8
	18.0	14.0	2.4	0.2		13	1.1
	13.0	26.0	19.0	0.6		17	1.5
28.	18.0	26.0	9.4	0.2		9.0	2.9
	15.0	20.0	5.2	0.4		11	1.8
	13.0	13.0	6.6	0.2		11	1.2
				2.6	30		
29.	6.8	6.6	8.6	1.4	25-30	12	0.55
30.	4.3	2.0	3.8	0.3		12	0.17
	14.0	27.0	3.6	0.4		14	1.9
31.	8.6	14.0	17.0	0.4		12	1.2
	9.7	33.0	50.0	0.7		12	2.8
	16.0	2.0	8.8	0.5		18	0.11
32.	13.0	9.4	7.2	0.2		14	0.67
	10.0	12.0	8.6	0.6		19	0.63
	16.0	2.2	8.9	0.4	20	7.7	0.29
	20.0	3.4	18.0	0.2		11	0.31
33.				1.1	10-15		
34.	14.0	23.0	44.0	0.4		14	1.6
	12.0	13.0	15.0	0.2		10	1.3
	12.9	23.0	52.0	0.4		14	1.6
	9.6	6.6	4.0	0.2		8.9	0.74
	6.8	5.4	3.6	0.4		12	0.45
	5.6	5.1	2.2	0.6		13	0.39
	12.4	10.0	6.2	0.4		17	0.59
35.				5.9	25-30		
36.				5.6	25-30		
37.				3.0	20-25		
38.	10.6	36.0	15.0	0.7	15-20	8.5	4.2 –
39.	9.5	16.0	14.0	1.3	≈ 20	14	1.1
40.	14.0	22.0	32.0	0.2		9.5	2.3
	16.0	13.0	4.8	0.1		8.5	1.5
	14.0	18.0	20.0	0.1		6.1	3.0

and constants from data in table 1.

9	10	11	12	13	14	15
	Φ	M	J/2	γ	$\sqrt{\rho g \cdot H/2}$	T
$\frac{2S_c}{Q_{35}}$	(equation 6) degrees	(equation 8) cgs units	(equation 10) cgs units	(equation 11) cgs units	(equation 12) cgs units	(equation 13) cgs units
0.54	30-35	18	13	0.010	120	170
1.3	35-40	28	18	0.015	180	290
0.49	30-35	17	9.7	0.005	83	200
0.20	20-25	12	5.8	0.005	71	100
1.0	30-35	29	14	0.006	120	320
0.73	30-35	27	11	0.011	110	170
0.52	35-40	8	12	0.014	120	320
0.24	25-30	8	7.1	0.007	75	110
0.72	35-40	13	13	0.015	140	280
0.18	30-35	5	8.9	0.010	93	130
1.1	35-40	23	11	0.012	110	260
1.0	35-40	28	18	0.020	190	230
0.47	35-40	9	12	0.012	120	220
0.60	30-35	19	12	0.009	110	180
0.72	30-35	25	12	0.004	90	220
0.30	15-20	20	7.2	0.001	47	120
0.26	35-40	6	18	0.015	180	340
1.4	35-40	44	19	0.008	150	340
4.2	40-45	32	28	0.014	240	680
0.49	30-35	11	1.0	0.010	11	22
0.51	25-30	21	9.0	0.006	82	130
0.45	30-35	13	9.8	0.006	87	220
1.2	35-40	36	2.0	0.019	20	23
1.6	$\approx$ 40	50	2.2	0.027	24	28
3.1	35-40	76	15	0.013	150	290
1.5	30-35	46	14	0.009	120	200
3.7	35-40	83	16	0.012	150	320
0.45	30-35	19	11	0.005	91	140
0.30	25-30	11	9.3	0.003	72	170
0.17	25-30	5	9.5	0.002	67	220
0.36	25-30	12	7.5	0.006	72	140
1.8	40-45	28	33	0.019	290	660
1.0	30-35	21	15	0.007	130	340
3.4	35-40	90	19	0.016	180	280
0.59	35-40	19	11	0.012	120	130
3.3	$\approx$ 40	112	22	0.018	210	230

Table 2.--Calculations, of velocities, strengths,

1	2	3	4	5	6	7	8
	Velocity	S_E (equation 3)	$2S_c$ (equation 2)	B	Φ_β (equation 2)	Q_{35} (equation 2)	$\frac{S_E}{Q_{35}}$
	m per sec	10^5 dynes per cm^2	10^5 dynes per cm^2	10^5 dynes per cm^2	degrees	10^5 dynes per cm^2	
41.				1.4	≈ 10		
42.				2.5	≈ 25		
				0.8	15-20		
43.				2.3	15-25		
44.				0.8	10-15		
45.				1.3	20-25		
				7.4	≈ 30		
				1.2	20-25		
				2.4	20-25		
46.				0.6	15-20		
	9.1	29.0	20.0	1.0	≈ 20	10	2.9
				0.9	≈ 20		
47.	18.0	64.0	82.0	1.0	≈ 15	12	5.3
	13.0	15.0	20.0	0.5	≈ 15	13	1.2
48.				3.4	20-25		
49.	11.0	16.0	11.0	1.1		37	0.43
	16.2	43.0	34.0	0.5		15	2.9
	12.6	33.0	26.0	0.7		15	2.2
50.				1.1	≈ 15		
51.				1.2	≈ 20		
52.	16.7	37.0	22.0	0.3		10	3.7
	18.5	25.0	5.0	0.3		15	1.7
	24.5	46.0	20.0	0.7		27	1.7
	28.8	32.0	7.0	0.3		17	1.9
	30.0	24.0	8.8	0.2		21	1.1
	28.8	25.0	11.0	0.3		21	1.2
	28.0	38.0	17.0	0.4		18	2.1
	30.9	30.0	18.0	0.3		19	1.6
53.	13.5	9.7	14.0	0.3		24	0.69
54.	10.4	11.0	3.2	0.5		16	0.69
	5.6	2.5	0.72	0.6		19	0.13
	6.6	3.4	1.5	0.4		15	0.23
55.	23.0	72.0	80.0	0.4		12	6.0
	20.0	36.0	14.0	0.4		16	2.2
	10.0	28.0	48.0	0.6		18	1.6
	16.0	18.0	13.0	0.5		29	0.62
	19.0	21.0	9.2	0.3		15	1.4
	17.0	34.0	1.6	0.4		13	2.6
56.	5.6	4.8	8.6	0.6	≈ 15	16	0.30
57.				1.6	≈ 15		
58.	12.0	14.0	6.2	0.4		20	0.70
59.	20.0	38.0	12.0	0.4		10	3.8
	16.0	24.0	13.0	0.3		12	2.0

and constants from data in table 1.

9	10	11	12	13	14	15
$\frac{2S_c}{Q_{35}}$	ϕ (equation 6) degrees	M (equation 8) cgs units	J/2 (equation 10) cgs units	γ (equation 11) cgs units	$\sqrt{\rho g \cdot H/2}$ (equation 12) cgs units	T (equation 13) cgs units
2.0	40-45	41	32	0.015	270	650
6.8	> 45	79	25	0.029	270	580
1.5	30-35	54	14	0.010	130	210
0.30	25-30	8	8.6	0.005	78	270
2.3	≈ 40	43	22	0.021	220	450
1.7	35-40	26	19	0.013	180	480
2.2	40-45	39	21	0.022	220	370
0.33	35-40	8	13	0.014	140	220
0.74	35-40	12	11	0.018	130	280
0.41	30-35	8	9.8	0.019	120	160
0.42	25-30	13	7.1	0.016	89	110
0.50	30-35	14	8.0	0.016	100	130
0.94	35-40	18	11	0.021	130	200
0.95	30-35	21	8.3	0.018	110	140
0.58	25-30	35	8.1	0.006	77	130
0.20	30-35	5	9.6	0.005	84	210
0.04	10-15	2	4.3	0.001	32	100
0.10	20-25	5	6.6	0.002	48	120
6.7	45-50	86	24	0.040	280	480
0.88	35-40	16	14	0.019	150	280
2.7	35-40	64	23	0.011	200	550
0.45	25-30	15	8.6	0.009	90	190
0.61	30-35	16	11	0.013	120	180
0.12	≈ 40	2	16	0.017	170	330
0.56	25-30	31	11	0.002	79	200
0.31	30-35	10	10	0.006	98	210
1.2	40-45	17	17	0.023	180	310
1.1	35-40	24	14		150	250

Table 2.--Calculations of velocities, strengths,

1	2	3	4	5	6	7	8
	Velocity	S_E (equation 3)	$2S_c$ (equation 2)	B	Φ_B (equation 2)	Q_{35} (equation 2)	$\frac{S_E}{Q_{35}}$
	m per sec	10^5 dynes per cm^2	10^5 dynes per cm^2	10^5 dynes per cm^2	degrees	10^5 dynes per cm^2	
60.	22.0	54.0	74.0	1.3		40	1.4
	27.0	116.0	36.0	2.4		41	2.8
	21.0	46.0	114.0	1.9		86	0.53
	27.0	52.0	60.0	1.1		55	0.95
	21.0	57.0	24.0	3.2		75	0.76
61.	8.6	4.8	3.0	0.2		11	0.44
	12.0	11.0	4.2	0.3		14	0.79
	15.0	12.0	7.4	0.3		18	0.67
62.	28.0	41.0	16.0	0.4		24	1.7
	28.0	52.0	32.0	0.3		16	3.2
	19.0	28.0	17.0	0.4		19	1.5
	18.0	41.0	20.0	0.6		17	2.4
	21.0	32.0	14.0	0.3		15	2.1
	18.0	15.0	10.0	0.2		17	2.4
	19.0	25.0	14.0	0.4		19	1.3
	17.0	19.0	5.6	0.3		6.1	3.1
	7.7	4.9	5.0	0.4		19	0.26
63.	15.0	13.0	2.8	0.1		8.3	1.6
	10.0	8.8	6.6	0.2		9.4	0.94
64.	16.0	11.0	3.8	0.1		8.8	1.2
	8.0	6.0	3.2	0.3		11	0.55
	15.0	20.0	3.4	0.2		7.9	2.5
65.				1.9	15-20		
66.	7.9	5.4	3.2	0.5	10	15	0.36
67.	13.0	5.6	3.4	0.3		18	0.31
	16.0	25.0	8.8	0.4		12	2.1

and constants from data in table 1.

9	10	11	12	13	14	15
	Φ	M	J/2	γ	$\sqrt{\rho g' H/2}$	T
$\frac{2S_c}{Q_{35}}$	(equation 6) degrees	(equation 8) cgs units	(equation 10) cgs units	(equation 11) cgs units	(equation 12) cgs units	(equation 13) cgs units
1.8	35-40	25	11		120	390
0.88	40-45	6	13	0.025	160	630
1.3	25-30	28	8.2	0.011	90	350
1.1	30-35	22	8.8	0.016	110	280
0.32	30-35	4	7.6	0.011	86	420
0.27	25-30	13	8.3	0.003	66	120
0.30	30-35	11	11	0.006	99	170
0.41	30-35	16	8.7	0.008	84	140
0.68	35-40	15	11	0.021	130	220
2.0	$\approx$ 40	37	15	0.030	190	270
0.89	30-35	22	12	0.014	130	240
1.2	35-40	18	16	0.018	200	370
0.93	35-40	21	14	0.020	150	240
0.59	30-35	22	9.4	0.010	99	140
0.75	30-35	17	11	0.013	120	220
0.92	45-50	11	12	0.008	120	190
0.26	20-25	15	8.0	0.003	61	140
0.34	30-35	12	13	0.011	130	150
0.67	30-35	26	12	0.006	100	170
0.41	30-35	15	10	0.010	100	120
0.29	25-30	14	11	0.004	88	160
0.43	35-40	9	16	0.014	160	240
- 0.21	25-30	8	7.3	0.003	61	140
0.19	15-20	9	5.1	0.003	48	79
0.73	35-40	13	14	0.013	140	270

using the sun angle and shadow length. Boulder shadow widths were measured when they were smaller near the base of the boulder than near the center. Boulder dimensions perpendicular to the sun direction were measured on the shadow image and on the boulder image while only the boulder image could be used in the other direction. Boulder heights were estimated using the shadow length and, where interpretation dictated, boulder heights included the depth of the track. The ranges to the secondary craters were estimated by measuring from the rim of the parent primary crater to the center of the secondary impact crater.

Boulder volumes were generally computed assuming a triaxial spheroid although when shapes were clearly rectangular the volumes were estimated using the appropriate dimensions. Boulder masses were computed using a density of 2.7 gm per cm^3. Volumes of secondary craters were calculated assuming a triaxial hemispheroid. Areas at the bases of boulders were taken as elliptical unless the geometry indicated otherwise. The axes for the elliptical bearing area were taken as the track width and minimum boulder width at right angles to the track measurement.

Velocities of blocks producing secondary impact craters were computed using the classical ballistics equation and assuming an ejection angle of 45°:

$$R = \frac{V^2 \sin 2\Delta}{g} \qquad (1)$$

where R is the range to the secondary crater

V is the velocity of the block

Δ is the ejection angle of the block

g is the acceleration of gravity at the lunar surface (163 cm per sec^2).

Locations, crater dimensions, block dimensions, track dimensions are listed in table 1. Values computed for block velocities, penetration resistances, bearing pressures, static friction angles, and coefficients for various low velocity impact craters are listed in table 2.

A summary of Surveyor results

Analyses of Surveyor data have evolved with time and certain problems are unresolved. As a result of an analysis of Surveyor I data, Jaffe (1967, p. 1727-1731) postulates: (1) a porous, fine-grained, particulate surface material that fails by local shear, (2) a cohesion of 10^2 to 10^5 dynes per cm^2, probably 10^3, (3) a change in density from 0.6-0.7 gm per cm^3 at the surface to 1.0 gm per cm^3 at 10 to 20 cm depth, and (4) a friction angle of about 55°. Surveyor I data (Christensen and others, 1967a, p. 813; O'Keefe and Scott, 1967, p. 1174) are also consistent with: a soil with a cohesion of 1.3×10^3 to 4.0×10^3 dynes per cm^2, a friction angle between 30° and 40°, and a density of 1.5 gm per cm^3. The difference between the two interpretations results from the failure modes assumed. For the 55° internal friction angle the failure is by local shear and for the 30°-40° friction angle the failure is by general shear.

Bearing tests using the 2.5 cm wide surface sampler on Surveyor III showed the surface is uplifted and disturbed to a distance of 10 to 12.5 cm indicating that the friction angle is at least 35° and that failure occurs by general shear (Scott, Roberson, and Clary, 1967, p. 85-88 and Scott and Roberson, 1968a, p. 4076). Preliminary results from studies of spacecraft landing interactions for Surveyor III placed the static bearing capacity of the lunar surface near 2×10^5 to 5.5×10^5 dynes per cm^2 (3 to 8 psi) and in the same range as that for Surveyor I. For a footing of Surveyor size (20 to 30 cm), these numbers correspond to an angle of internal friction near 45° to 60° for a cohesionless soil. If the soil is assumed to be frictionless the calculated cohesion is near 1.0×10^5 dynes per cm^2 (Christensen and others, 1967b, p. 119-120; Christensen and others, 1968a, p. 4091). Additionally, footpad imprints indicate the material is very fine grained.

Preliminary analysis of Surveyor V data show the resistance to bearing load there is less than for the other Surveyor sites (Christensen and others, 1968b). Such apparent weakness can be accounted for by the slope upon which it landed (Karafiath and Nowatzki, 1968). Additionally, analysis of the soil reaction to the vernier engine exhaust gases placed the grain size of the lunar surface materials in the 2 to 60 micron size range, in general agreement with footpad imprint analyses.

Analyses of the soil reaction at the Surveyor VI site during vernier engine firing place the lower limit on the cohesion of the materials at 7×10^2 dynes per cm^2 when the density is taken as 1.5 gm per cm^3 and the friction angle is taken as 35°; and, analyses for the altitude control jets yield estimates of 0.5×10^4 to 1.7×10^4 dynes per cm^2 (Christensen and others, 1968c).

The soil properties at Surveyor VII, a highland site with a large population of large rocks, are similar in general to those of the other Surveyor sites (Choate and others, 1968) but less brittle (Scott and Roberson, 1968b). The density of a rock picked up by the surface sampler on Surveyor VII was in the range of 2.4 to 3.1 gm per cm^3 (Scott and Roberson, 1968b). One small rock drop test was made during the Surveyor VII mission (Choate and others, 1968, p. 101-107) which yields an upper bound dynamic penetration resistance of 3.1×10^5 dynes per cm^2.

A summary of the Surveyor program results by the Mechanical Properties team (Choate and others, 1969, p. 167) shows the lunar surface materials: (1) are very fine grained (2 to 60 micron range) with permeabilities like those of terrestrial silts, (2) have a cohesion between 7×10^2 and 1.2×10^4 dynes per cm^2, (3) increase in strength with depth, and (4) have a bearing capacity of about 4×10^5 to 6×10^5 dynes per cm^2 using footpad (20 to 30 cm diameter footing) analyses at a depth of 4 to 6 cm. The Lunar Surface Sampler team (Scott and Roberson, 1969a, p. 178) concludes that: (1) the surface materials at the Surveyor III and

VII sites at a depth of several centimeters are consistent with a material possessing a cohesion of the order of 0.35×10^4 to 0.7×10^4 dynes per cm^2, an angle of internal friction of 35° to 37°, and a density of about 1.5 gm per cm^3, (2) the uppermost several millimeters of the lunar surface materials appear to be less dense, softer, and more compressible than underlying materials, (3) the density of a rock, picked up and weighed by Surveyor VII, is between 2.4 and 3.1 gm per cm^3, and (4) the surface materials are predominantly fine grained, granular, and slightly cohesive.

Boulder tracks--Results

Estimates of static bearing capacities computed for 48 boulders indicate mean and median friction angles near 17° and 17.5° with a range of 10° to 30° (see fig. 3 and table 2, columns 3 and 4). Such estimates employ Terzaghi's bearing capacity equation for circular footings (Terzaghi, 1948, p. 125; Scott, 1963, p. 440-449):

$$Q = 1.3\ N_c\ C + {}_0gN_q\ D_f + 0.6\ {}_0gN_\nu\ R_f \qquad (2)$$

where: Q is the bearing capacity in dynes per cm^2,

N_c, N_q, N_ν are dimensionless numbers for general shear conditions (these numbers are a function of friction angle and slope angle),

C is the cohesion (taken as 10^3 dynes per cm^2)

ρ is the density of the soil-like material (taken as 1.35 gm per cm^3),

g is the acceleration of gravity at the lunar surface (taken as 163 cm per sec^2),

D_f is the depth of footing in centimeters (generally taken as the depth of track nearest the boulder),

R_f is the radius of footing in centimeters.

Dimensionless numbers for level surfaces are taken from Meyerhof (1951) and boulder masses are computed as outlined in the previous section on Methods and Procedures.

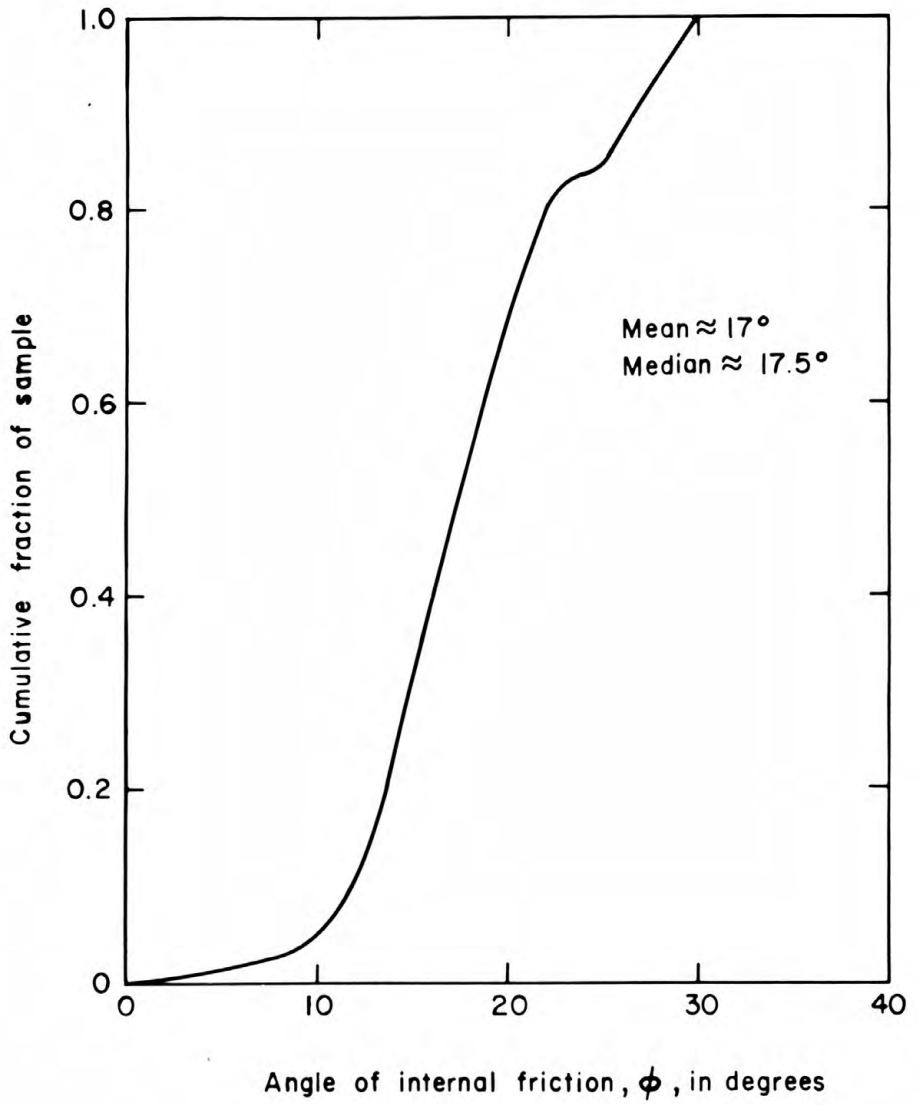

Figure 3.--Cumulative frequency distribution of friction angles based on data computed for 48 boulder tracks.

Angles of internal friction were obtained as follows: (1) the estimated bearing pressure (B), which is the product of the mass of the boulder and the acceleration of gravity divided by the bearing area, was calculated (see table 2, column 5, item B), (2) the bearing capacity, Q, was calculated using values of N_c, N_q, and N_γ for angles of internal friction in 5° steps combined with values for footing depth, radius, and a cohesion of 10^3 dynes per cm^2 until the calculated value of Q corresponded to or bracketed the estimated bearing pressure. When the calculated value of B bracketed the bearing pressure, the 5° interval of friction angles was recorded (see table 2, column 6, item Φ_B). Values used for boulder masses, footing depths, and footing areas for each boulder can be found in table 1, under the headings of (1) Block mass and (2) Track depth and area. Footing radii were calculated as the square root of the bearing area times $1/\sqrt{\pi}$ when the bearing area was taken as ellipsoidal.

The friction angles of 10° to 30° computed by the above method are substantially lower than the 35°-37° angles obtained by the lunar surface soil sampler (Scott and Roberson, 1969) suggesting that these are either significant variations in the mechanical properties of the lunar surface materials or the method is inadequate for precise determinations of the mechanical properties of the lunar surface materials. The differences are further accentuated when the cohesion is taken as 10^4 dynes per cm^2 instead of 10^3 dynes per cm^2 and the density of the soil is taken as 1.5 gm per cm^3 instead of 1.35 gm per cm^3 (see Choate and others, 1969; Scott and Roberson, 1969). Such changes would reduce the estimated friction angles by about 4° to 5°. The effects of varying the parameters in equation 2 are shown in the following calculation. For a 1 m radius footing at a depth of 0.25 m on a soil failing by general shear with a friction angle of 35°, a cohesion of 10^3 dynes per cm^2 and a density of 1.35 gm per cm^3,

the static bearing capacity is:

$$Q = 9.28 \times 10^5 \text{ dynes per cm}^2.$$

If the cohesion is increased to 10^4 dynes per cm^2 and the density of the bearing material is increased to 1.5 gm per cm^3, the friction angle is reduced to between 30° and 31°:

$$Q = 9.28 \times 10^5 \text{ dynes per cm}^2$$

$$= 1.3\,(N_c)\,10^4 + 1.5\,(163)\,(N_q)\,(25) + 0.6\,(1.5)\,(163)(N_\gamma)\,(100)$$

and $41 > N_c > 37$, $24 > N_q > 22$, $24 > N_\gamma > 20$; for which

$31° > \Phi > 30°$, where Φ is the angle of internal friction.

On the other hand some authors have reasoned the areas beneath the boulders are half as large as those used in this report (see for examples, Hovland and Mitchell, 1969; Felice, 1967; Eggleston and others, 1968). In their analysis, they argue that the rear half of the boulder base is exposed to free space. Such a reduced footing has an effect of about 5° on computed friction angles. In any event, the friction angles obtained are considerably less than those estimated from Surveyor spacecraft data.

Other workers (Hovland and Mitchell, 1969) report friction angles between 25° and 45° for boulders shown on Lunar Orbiter V photographs. In their analyses they assume: (1) the boulders are spherical, (2) soil density is 1.6 gm per cm^3, (3) boulder densities are 2.7 gm per cm^3, (4) and the cohesion is 10^3 dynes per cm^2. The mean value for their friction angles is 33.7°, in fair agreement with Surveyor results. In their discussion they point out the need to account for the effect of slope on the dimensionless numbers (see Meyerhof, 1951). Slope angles were not considered here since attempts to measure slope angles using photoclinometric and photogrammetric techniques did not yield satisfactory results. Several tracks and boulders were not analysed because they were on steep slopes.

Data on low velocity impacts

Before proceeding to estimates of the mechanical properties of the lunar surface using secondary impact craters, a brief discussion of low velocity impact data, theory, and equations is desirable. Estimates of mechanical properties of a target material using non-instrumented projectiles requires that projectile properties and the geometry of the secondary crater and boulder be used. Projectile mass, cross-sectional area, velocity, and shape are commonly used projectile properties. Results of the impacts are commonly described in terms of penetration depth, crater volume, and crater diameters. Penetration depth is the result most commonly used.

Euler's equation (Goldsmith, 1960, p. 298, equation 6.11) can be used to define an apparent strength (S_E) using the depth of penetration (P), the velocity of the projectile (V), the projectile mass (m), and the cross-sectional area of the projectile at right angles to the velocity vector (A):

$$S_E = \frac{mV^2}{2AP} \qquad (3)$$

Here the assumption is made that force of resistance per unit area is constant throughout penetration.

Charters and Summers (1959) use crater volume (Vo) and one-half the kinetic energy of the projectile to define an apparent strength (S_c):

$$S_c = \frac{mV^2}{4Vo} \qquad (4)$$

They assume the crater is a hemispherical expanding cavity, the strength is constant, and one-half the kinetic energy is lost in motion of the accelerated masses.

The Poncelet equation assumes the force resisting penetration (f) is of the form:

$$f = \alpha + \beta V^2 \qquad (5)$$

where α is a constant term and β is an inertial term. Penetration, mass per unit area, and projectile velocity are then used to evaluate the constant to find the constants in the Poncelet equation (Goldsmith, 1960, p. 298, eq. 6.12; Nara and Denington, 1954, p. 20):

$$P = \frac{m}{2A\beta} \ell n\left(1 + \frac{\beta}{\alpha} V^2\right) \qquad (6)$$

Nara and Denington (1954, p. 31-34) interpret the Poncelet equation for soil by noting that $f/A = \alpha$ when V equals zero which, in turn, implies α is the static bearing capacity (Q). βV^2 represents the force required to move fractured material from the path of the projectile. Nara's experimental constants for 3 g steel spheres are listed in table 3, with the bearing capacity, Q (using D_f at one-half maximum penetration).

Table 3.--Experimental constants for the 3 g spheres and bearing capacity, Q (Nara and Denington, 1954)

Name of Target (Nara, and Denington, 1954)	Soil constant $\alpha \left(\frac{\text{dynes}}{\text{cm}^2}\right)$	Inertial constant $\beta \left(\text{gm/cm}^3\right)$	Bearing capacity $Q \left(\frac{\text{dynes}}{\text{cm}^2}\right)$	Cohesion C	Angle internal friction Φ
Eglin Sand	1.3×10^6	0.88	3.7×10^6	0	31
Portage Sand	0.25×10^6	1.1	4.6×10^6	0	30
East Lake Clay 1	5.6×10^6	0.56	6.8×10^6	0.27×10^6	21
East Lake Clay 2	$31. \times 10^6$	0.12	33×10^6	0.54×10^6	23
East Lake Clay 3	$38. \times 10^6$	0.14	44×10^6	0.81×10^6	21
Chester Clay	$41. \times 10^6$	0.34	44×10^6	0.75×10^6	27
Neff Clay 1	$170. \times 10^6$	0.04	180×10^6	3.0×10^6	--
Neff Clay 2	$240. \times 10^6$	0.25	220×10^6	4.0×10^6	24

If Nara's interpretation is correct, $\alpha(=Q)$ is a function of penetration, P, and equation 5 does not follow from equation 4. Correct integration (Albert Chen, written commun.) yields:

$$P = \frac{m}{2A\beta} \ell n \left(\frac{1.3\, N_c\, C + 0.6\, \rho g\, N_\gamma\, R_f + \rho g\, N_q \frac{m}{2A\beta} + \beta V^2}{1.3\, N_c\, C + 0.6\, \rho g\, N_\gamma\, R_f + \rho g\, N_q \frac{m}{2A\beta} + \rho g\, N_q P} \right) \qquad (7)$$

P = penetration

m = projectile mass

A = projectile crossectional area

β = a constant, inertial

N_c, N_γ, N_q = dimensionless soil constants

ρ = soil density

C = soil cohesion

R_f = radius of projectile cross section

g = acceleration of gravity

A depth dependence has been observed by Nara and Denington (1954a, p. 13, 14) for 3.5 cm diameter cylindrical projectiles weighing 243 and 456 grams fired with horizontal trajectories into cohesionless sand targets with normal incidence at depths of 30.5 and 61 cm. Horizontal penetrations were reduced 0.635 and 1.14 cm by this change in overburden. This decrease in penetration with increasing overburden pressure is in approximate quantitative agreement with predictions using soil mechanics data. For Nara's data (1954) on penetration of 3 g spheres impacting on cohesive targets with normal incidence of clay at velocities between 15 to 457 m per sec, equation 5 can be used instead of equation 6, where α is equal to the cohesive term ($1.3\, N_c C$) of the static bearing capacity equation (equation 2).

Studies of low velocity impacts with sand in an atomosphere

of air at velocities between 2 and 1000 m per sec (Mortensen, 1967; Cook and Mortensen, 1967) indicate that crater sizes are dependent on grain size of the target materials. Mortensen (1967) fits his data with equations of the form:

$$\frac{\frac{1}{2}\ mV^2}{(\frac{m}{A})\ Vo} = M(V)^{0.8} \qquad (8)$$

where: M is the coefficient dependent on particle size. Although Mortensen concludes crater size is proportional to the grain diameter, his data show it is more nearly proportional to the square root of grain diameter. Coefficients for Mortensen's (1967, p. 67) data are listed in table 4. In addition, the approximate coefficient, M, obtained from data on the impact of 9.44, 16.30, and 21.40 cm diameter cement spheres at normal incidence with velocities between 1 and 10 m per sec is listed in table 4.

Table 4.--Coefficients in the Mortensen (1967) equations (equation 8) as a function of grain size

Mesh	Mean grain size (mm)	M
-14 + 20	1.0	86.4
-28 + 48	0.44	109.8
-60 +100	0.178	210.0
--	0.3	≈358.0[1/]

[1/] Coefficient for cement spheres.

Empirical studies of low velocity impacts of small spheres into 32 μ to 600 μ particulate matter in vacuum (Hanks and McCarty, 1966; Clark and McCarty, 1963) indicate that equations of the form:

$$P = \frac{k\, m^{\frac{1}{2}}\, V^{2/3}}{d} \tag{9}$$

where K is a constant and d is the projectile diameter, can be used to predict low velocity penetration. Equation 9 can be recast to give

$$J = \frac{mV^2}{AP} \cdot \frac{1}{V^{4/3}} \cdot \frac{1}{\left(\frac{m}{A}\right)^{\frac{1}{2}}} \tag{10}$$

where J is a constant using their value for k of 0.44 from data collected under vacuum conditions and for particle sizes between 32 μ and 600 μ (Clark and McCarty, 1966, p. 10), J becomes 55.2 (cgs units). For the cement spheres mentioned previously J is about 54 to 80 (cgs units). For Mortensen's data, the values of J are between 30 and 100 and probably average near 40 to 50. For unpublished data for 1 inch steel spheres impacting sand at 1.4 to 2.8 m per sec, J is about 50 to 54 (Peter Coffin, written commun.). Additionally, equation 9 is in good agreement with the data of Pyrz (1969).

The Sandia Corporation (Young, 1967) developed an empirical equation for the penetration of large slender rods impacting with velocities less than 60.1 m per sec. Their results can be expressed:

$$\gamma = \frac{N}{AP} \left(\frac{m}{A}\right)^{\frac{1}{2}} \ell n \left(1 + \frac{V^2}{4.64 \times 10^7}\right) \tag{11}$$

where γ is a coefficient related to the soil, N is a nose shape factor, and all dimensions are in cgs units. Values for N are 0.56 for a flat nose projectile and 1.08 for a conical nose with a diameter-altitude ratio of 2. Approximate values of γ for their data (Young, 1967) are given in table 5 along with their

soil designation and coefficients.

Table 5.--Coefficients for the Sandia Corporation penetration equation (Young, 1967)

Material	Sandia Code	Sandia Soil coefficient	Y
Silty clay, soft, very wet	ST, SC, M	40-50	0.009-0.01
Sand, loose, moist	SA, DA	4.4 - 6.5	0.04 -0.07
Clayey silt, dense, hard	DL	5.2	0.09 -0.11
Gypsum, lake beds, hard, moist	GY	2.5	0.15 -0.22
Rock, sandstone	SS, R	1.07 - 1.3	0.3 -0.4

Moore (1967b) suggested a penetration equation of the form:

$$H = \left(\frac{m}{A}\right)^{\frac{1}{2}} \frac{V}{(\rho g)^{\frac{1}{2}} P} \qquad (12)$$

where H is a coefficient for sand targets, based on data using small brass rods. For his data $(\rho g)^{\frac{1}{2}}H$ equals 1450 in cgs units; and, for the Moon with g = 163 cm per sec^2 and ρ = 1.35 gm per cm^3, $(\rho_t g)^{\frac{1}{2}}H = 526$.

Finally, the data on the impact of cement spheres into 0.3 mm sand indicate the data should be normalized using the following equation (Moore and Hawley unpub. data):

$$\frac{S_E}{V_n^{1.3}} = T \qquad (13)$$

where T is a coefficient between 151 to 207 and averages about 180.

The acceleration of gravity has a demonstrable effect on the penetration of rods into coarse sand (Ottawa sand) and penetrations for the Moon will be at least 1.18 to 1.28 times larger on the Moon than on the Earth (Pyrz, 1969). Using the data and equations of Pyrz (1969, from figure 8, p. 35) one concludes

$$\frac{P_m}{P_e} = \left(\frac{g_e}{g_m}\right)^{0.14} = 1.28; \qquad (14a)$$

and, from equation 16 (Pyrz, 1969, p. 42):

$$\frac{P_m}{P_e} = 1.18, \qquad (14b)$$

where: P_{m/P_e} is the ratio of penetrations on the Moon and Earth for coarse sand and for a given set of projectile properties. The effects of the atmosphere were not analyzed by Pyrz and it is possible that P_{m/P_e} could be as large as 1.4 to 1.56 (Johnson and others, 1969, p. 4848-4849, Chabai, 1965).

Angle of impact and penetration

Data on reduced penetrations resulting from decreasing angles of impact are scarce for low velocity projectiles. For oblique impacts of small spherical projectiles with powdered silty clay, the ratio of penetration and the normal component of velocity is nearly independent of angle of impact when impact angles are larger than 45° or so and projectile velocities are near 10 to 20 m per sec (Mitchell and others, 1969).

Data on reduced volumes of craters resulting from oblique impact are also scarce. For hypervelocity impacts, the energy per unit volume is inversely proportional to the cosine of the impact angle measured from the vertical or the sine of the angle measured from the horizontal (Bryan, 1962). Approximately the same results are obtained for impacts of lexan projectiles at 1 km per sec with sand when angles of impact are larger than about 15° (Gault and other, 1965, p. 129, fig. 6-5). On the other hand, earlier workers report that crater volume is inversely proportional to the cosine of the angle of impact measured from the normal for the impact of lead pellets with lead targets (Partridge and VanFleet, 1958). Thus, data on the effect of the angle

of impact are not only scarce but also conflicting.

The procedure used in the following section on lunar secondary impact craters will be to use the normal component of velocity in all penetration equations and volumes of craters will be corrected for the sine of the angle of impact. Errors introduced by this procedure are believed to be comparable to or less than other possible errors. For example, the product of the sine of 45° and the square of the velocity is 1.41 times larger than the square of the normal component of velocity for a 45° impact angle; and, when the impact angle is 60° the factor is 1.16. This is comparable to other effects such as nose shape (Young, 1967) for which hemispherical projectiles may penetrate 1.29 times further than flat nose projectiles. Additional uncertainties of 1.41 can be introduced by the unknown orientations of elongate blocks when their lenth-width or length-height ratios are 1.41.

Secondary impact craters--Results

For each secondary impact crater, most of the equations discussed above are used to estimate the mechanical properties of the lunar surface. Solutions to the equations yield values that are more or less consistent with Surveyor data and terrestrial data after making appropriate corrections for factors related to the acceleration of gravity. The data used are listed in tables 1 and 2 where the density of the block was taken as 2.7 gm per cm^3 and ejection angles were assumed to be 45°. Analyses of the data suggest that ejection angles near 60° to 70° would be more realistic.

Euler's equation (equation 3) yields numbers comparable to those reported by the Surveyor project when the normal component of velocity is used (i.e., V_n^2). Solutions of equation 3 are listed in table 2, column 3. For dynamic strengths computed in this way, the mean value for the sample is 25.2×10^5 dynes per cm^2 (37 psi) and the median value is near 20.0×10^5 dynes per cm^2

(29 psi). Eighty-four percent of the sample exceeds a value of 7.1×10^5 dynes per cm^2 (10 psi) and 16 percent is larger than 41.0×10^5 dynes per cm^2 (60 psi). The use of the velocity (i.e., V^2) and a sine θ correction for the penetration length instead of the normal component of velocity would increase these values by $\sqrt{2}$.

Comparison of the values of penetration resistance obtained with the Euler equation (equation 3) and static bearing capacities for each block using angles of internal friction of 30° (Q_{30}), 35° (Q_{35} table 2, column 7) and 40° (Q_{40}) and the same assumptions used for the boulder tracks show the magnitude of the Euler values compare well with the Surveyor program results. Computed ratios of the Euler penetration resistance and static bearing capacity using a friction angle of 35°, a footing radius equal to the square root of the horizontal radii of the block, and crater depth for footing depth, average 1.6 and the median is 1.3 (fig. 4). These numbers correspond to, roughly, friction angles of 38° and 36°. About 84 to 89 percent of the ratios of the sample exceed the expectations for 30° friction angles. The scatter of the data, measured using the ratio of values of the abscissa in figure 4 at 16 and 84 percent, is about 5.3. Such a comparison of penetration resistance and static analyses ignore the dynamic effects of penetration resistance related to velocity. This will be discussed later.

For equation 4, the value of $2S_c$ is used instead of S_c using the argument developed by Scott and Jaffe (1966). In contrast with Charters and Summers (1959), Scott and Jaffe argue that only a small and negligible fraction of the initial kinetic energy of the impacting projectile reappears in the motion of the deforming soil. Here again, the numbers are roughly consistent with Surveyor program results. The mean value of $2S_c$ is 19.2×10^5 dynes per cm^2 (28 psi) and the median value is near 11.4×10^5 dynes per cm^2 (16.8 psi). Eighty-four percent of the sample

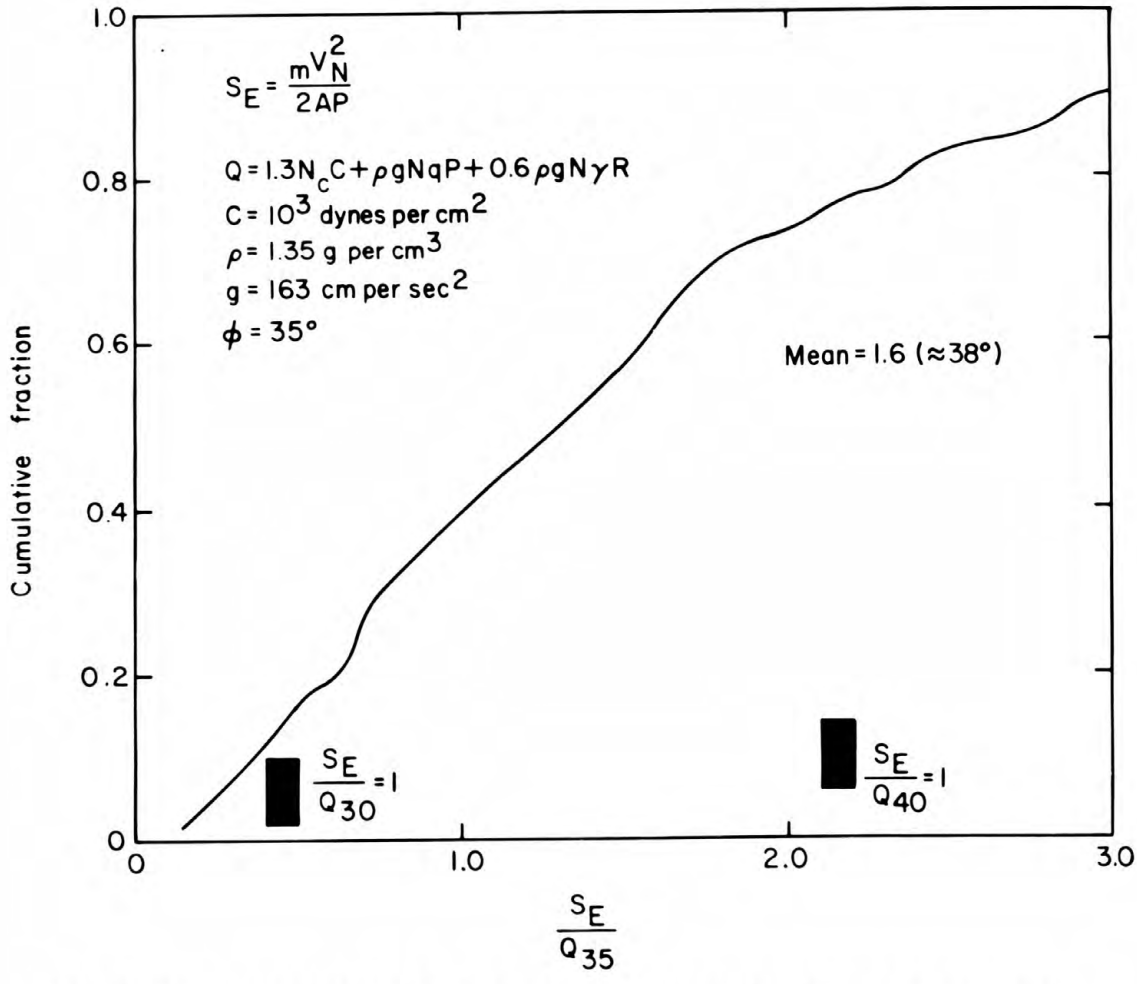

Figure 4.--Comparison of the ratio of dynamic strength computed using the Euler equation (S_E) and static bearing capacity for a friction angle of 35°(Q_{35}). Approximate position for ratios of S_E and static bearing capacities for friction angles of 30° (Q_{30}) and 40°(Q_{40}) are indicated where these ratios are equal to unity.

exceeds 3.6×10^5 dynes per cm^2 (5.3 psi) and 16 percent exceeds 32.0×10^5 dynes per cm^2 (47 psi). For this computation, the correction used for the angle of impact is the sine of the assumed ejection angle.

Comparison of the values of $2S_c$ (twice equation 4; see also table 2, column 4) with the static bearing capacity (Q_{35}), as above, yields a mean value near 1.15 and a median near 0.71 (see fig. 5). The values correspond to friction angles near 36° and 32°. About 63 to 75 percent of the ratios for the sample correspond to static bearing capacities for friction angles 30° (Q_{30}) and larger. Velocity dependent contributions to penetration resistance have been ignored in these calculations.

The simplified form of the Nara equation (equation 6, see also table 2, column 10) yields a mean and median friction angle of 34.4°. About 84 percent of the friction angles exceed 28.5° and 16 percent are larger than 40.5° (see fig. 6). For this calculation the following assumptions are made: (1) the normal component of velocity is used (i.e., V_n^2), (2) the value of β is 1.0 gm per cm^3, which is consistent with his data for sand and (3) the other values are the same values as used for the boulder tracks.

Thus, at this point the data seem to be in approximate agreement with Surveyor data. Problems arise, however, when one considers the velocity contributions to penetration resistance and when one tries to normalize the lunar data using terrestrial experimental data. For the previous cases the ratio of the values in terms of strength at the 16 and 84 percentile are, roughly: (1) 5.3 for the ratio of the Euler strength (S_E) and static bearing capacity for a 35° friction angle (Q_{35}), (2) 6.4 for the ratio of $2S_c$ and the static bearing capacity for a 35° friction angle (Q_{35}) and (3) approximately 5.0 for Nara's equation. It is possible to reduce this ratio and hence the scatter in the data to about 2.25 using other equations. Such a reduction in scatter of the data implies that a more correct equation has been

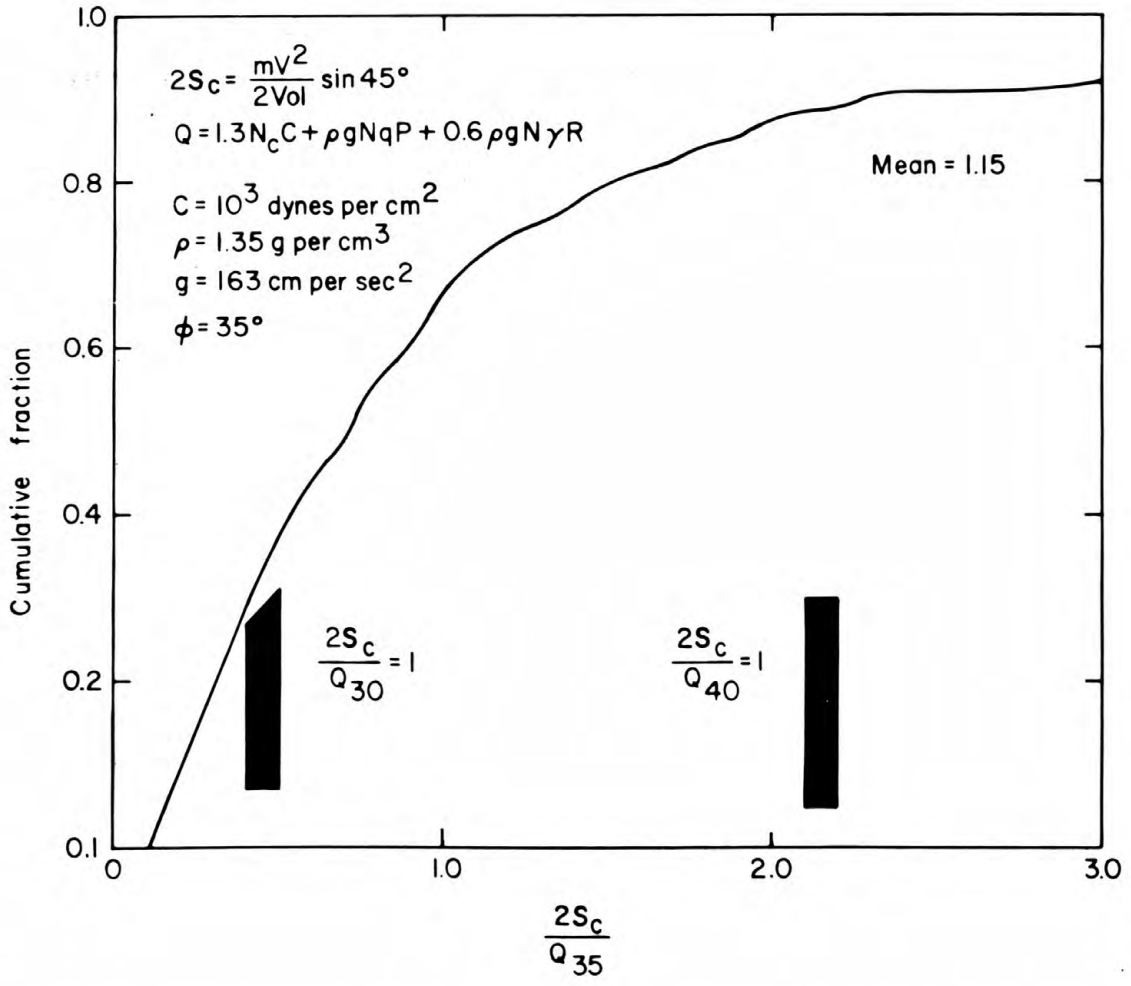

Figure 5.--Comparison of the ratio of the dynamic strength computed using the modified Charters and Summers equation ($2S_c$) and static bearing capacity for a friction angle of 35° (Q_{35}). Approximate position for ratios of $2S_c$ and static bearing capacities for friction angles of 30° (Q_{30}) and 40° (Q_{40}) are indicated where these ratios are equal to unity.

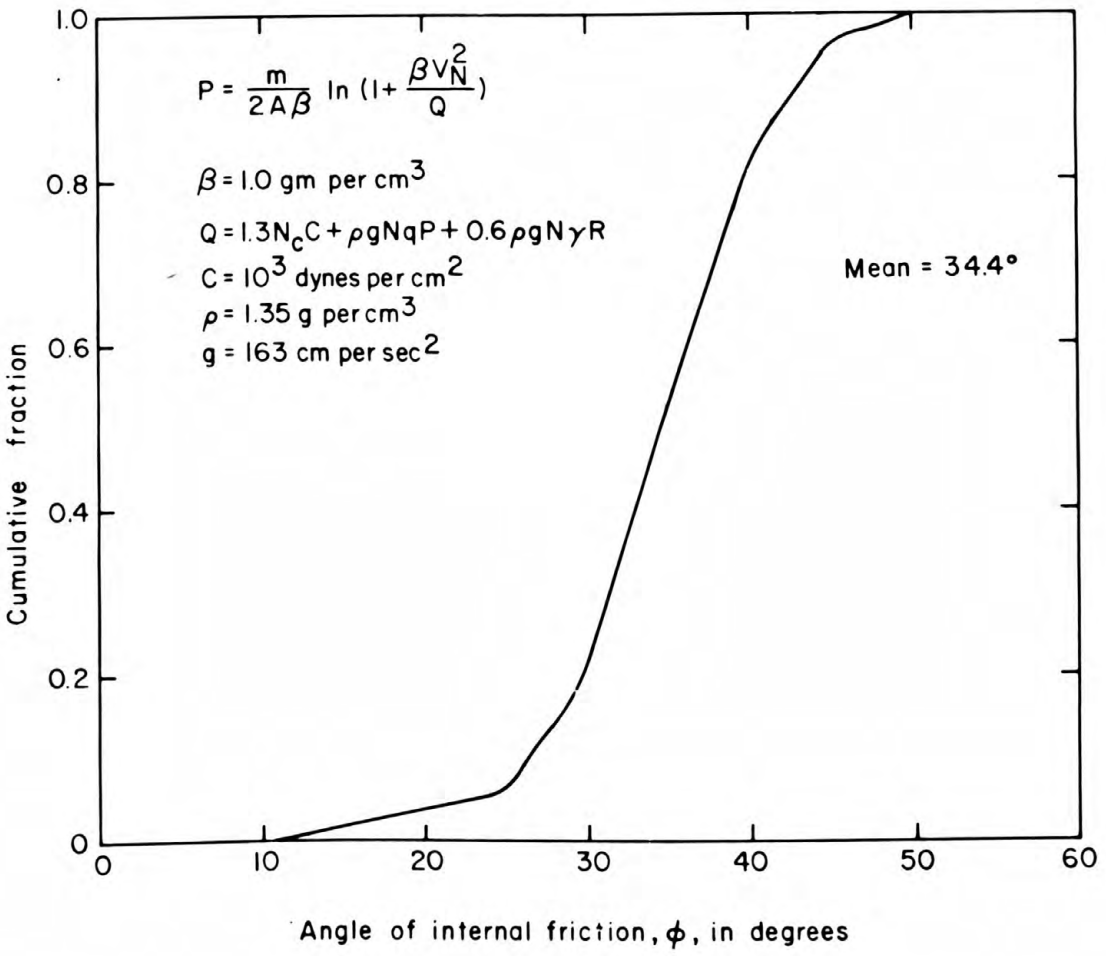

Figure 6.--Cumulative frequency of friction angles computed for secondary impact craters using the Nara simplified equation (equation 6) and assuming an ejection angle of 45°.

used with the data.

Mean and median values of M (equation 8, see also table 2, column 11), which is

$$M = \frac{2S_c}{\frac{m}{A} V^{0.8}} \qquad (15)$$

are 17.4 and 12.4 and the ratio of values at the 16 and 84 percentiles is near 5.4 (see fig. 7). Using this equation, scatter in the data is a slight improvement on the scatter in number 2 above. Also the mean value is significantly less than the terrestrial values of M for sand. The results can be improved by postulating that crater volumes on the Moon should be $(1.4)^3$ times larger than those on Earth (Johnson and others, 1969) because of differences in acceleration of gravity, and the corrected mean value becomes about 48. Using the analysis of Chabai (1965), the corrected mean value of M for the lunar acceleration of gravity could be about 66. Comparison with the terrestrial values of M equal 86.4 for the coarsest sand, a case where pore pressures should be of negligible importance, show that the corresponding lunar values are low.

The Clark and McCarty equations (equations 9 and 10) yield values of J equal to 55.2 for terrestrial experimental data. For the lunar data, the appropriate comparison is with the terrestrial value of J/2 or 27.6. Mean and median values of

$$J/2 = \frac{S_E}{V_n} \quad 1.33 \quad \left(\frac{m}{A}\right)^{\frac{1}{2}} \qquad (16)$$

for the lunar data are 13.35 and 11.2 (fig. 8; table 2, column 12). The ratio of the value of J/2 at the 84 and 16 percentiles is about 2.25 which represents a substantial reduction in the scatter of the data. Here again, lunar values for J/2 are less than those for terrestrial data. Corrections to the mean value for gravitational effects yield 17.1 (Pyrz, 1969), 18.8 (Johnson and others, 1969), and 20.9 (Chabai, 1965). The values still are

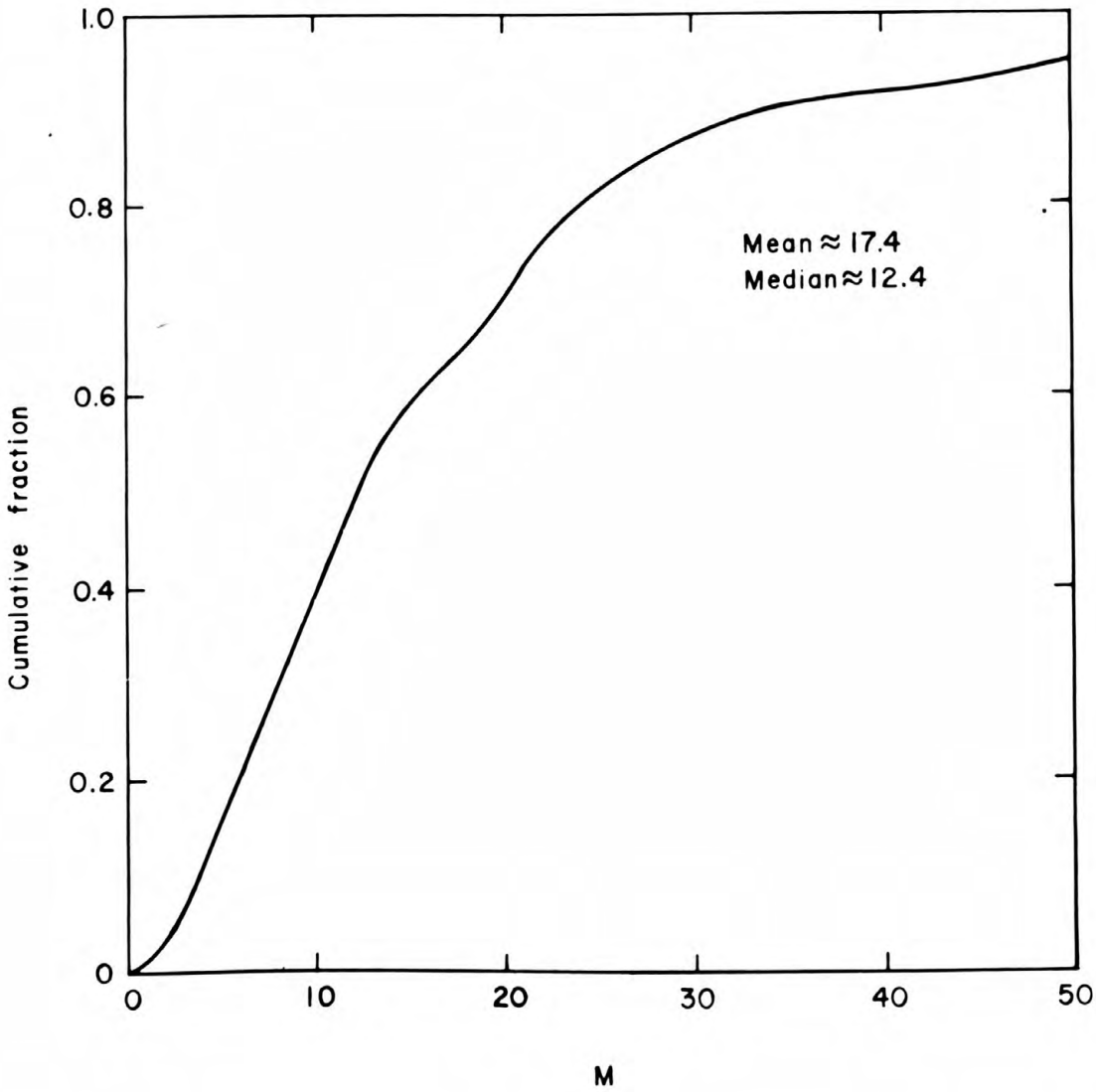

Figure 7.--Cumulative frequency of values of M (equation 10) for lunar data on secondary impact craters and assuming an ejection angle of 45°.

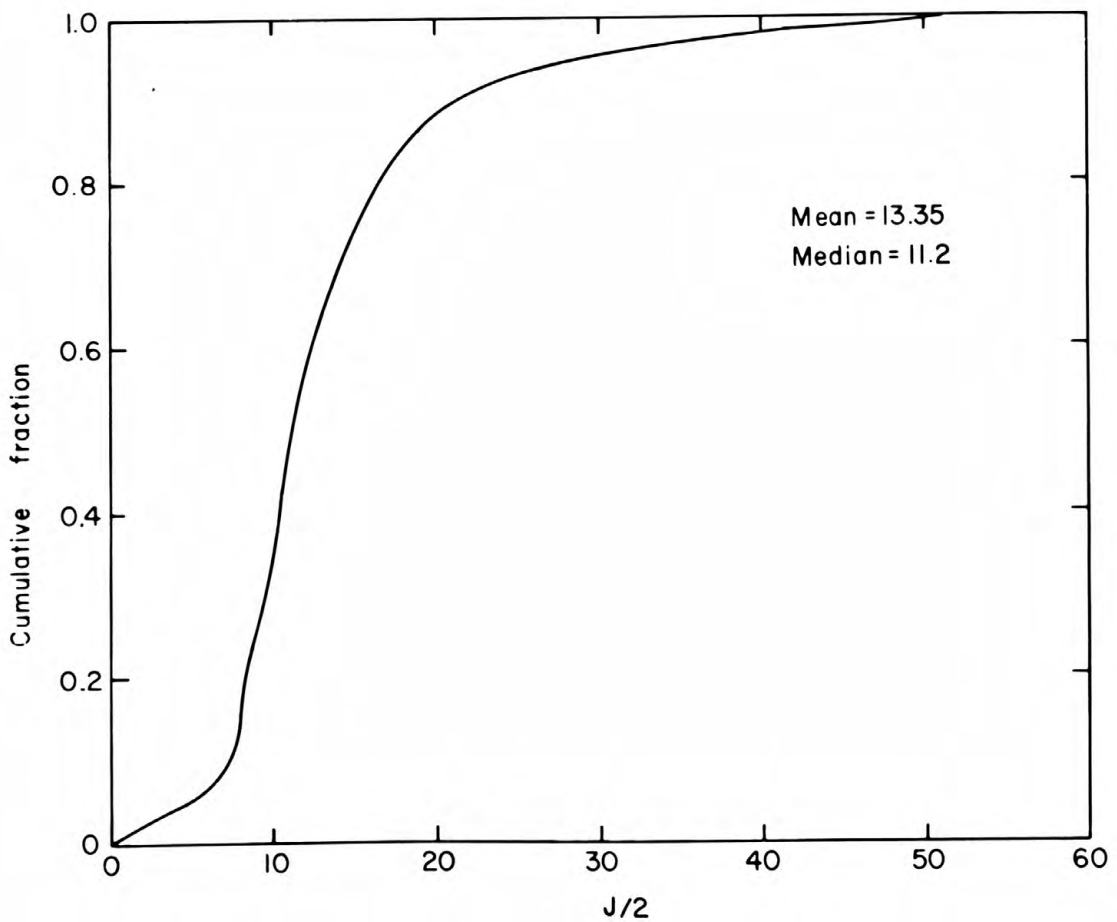

Figure 8.--Cumulative frequency of values of J/2 (equation 10) for lunar data on secondary impact craters and assuming an ejection angle of 45°.

lower than the value expected from terrestrial data.

An equation of the form of Moore (equation 12) reduces the scatter of the data considerably. Mean and median values of

$$\frac{S_E}{V_n} \left(\frac{m}{A} \right)^{\frac{1}{2}} \qquad (17)$$

are 131 to 115 and the ratio of these values at the 84 and 16 percentiles is 2.3 (fig. 9; table 2, column 14). Again, the mean and median values are much lower than would be expected from terrestrial data. For small rods into sand, values of equation 17 are near 646 to 725; and, for the cement spheres, these values were not constant but are between 135 to 361. Mean values computed from the lunar data and adjusted for gravitational effects could be as large as 168 (see Pyrz, 1969), 183 (see Johnson and others, 1969), 204 (see Chabai, 1965), and 294 (see Moore, 1967b).

The terrestrial experimental data on cement spheres can be correlated using equation 13 where this value is between 151 and 207 and averaging 180. Mean and median values for the lunar data are 290 and 220 (see figs. 10 and 11, and table 2, column 15) and the ratio of values at the 84 and 16 percentiles is about 2.75. Here, lunar data are comparable to terrestrial data.

Finally, attempts to use the Sandia equation have resulted in very low numbers for their coefficients. The average value of γ in equation 11 (see also table 2, column 13) is near 0.012 suggesting the lunar materials behave somewhat like soft-wet silty clay. Adjustments for gravitational acceleration to the average value of this coefficient for the Moon yields 0.015 (Pyrz, 1969), 0.017 (Johnson and others, 1969), 0.019 (Chabai, 1965), and 0.027 (Moore, 1967b).

Discussion of results

There are several reasons for considering that the assumed ejection angle of 45° is too low: (1) the penetration resistances computed with equations 3 and 4 compare too closely with

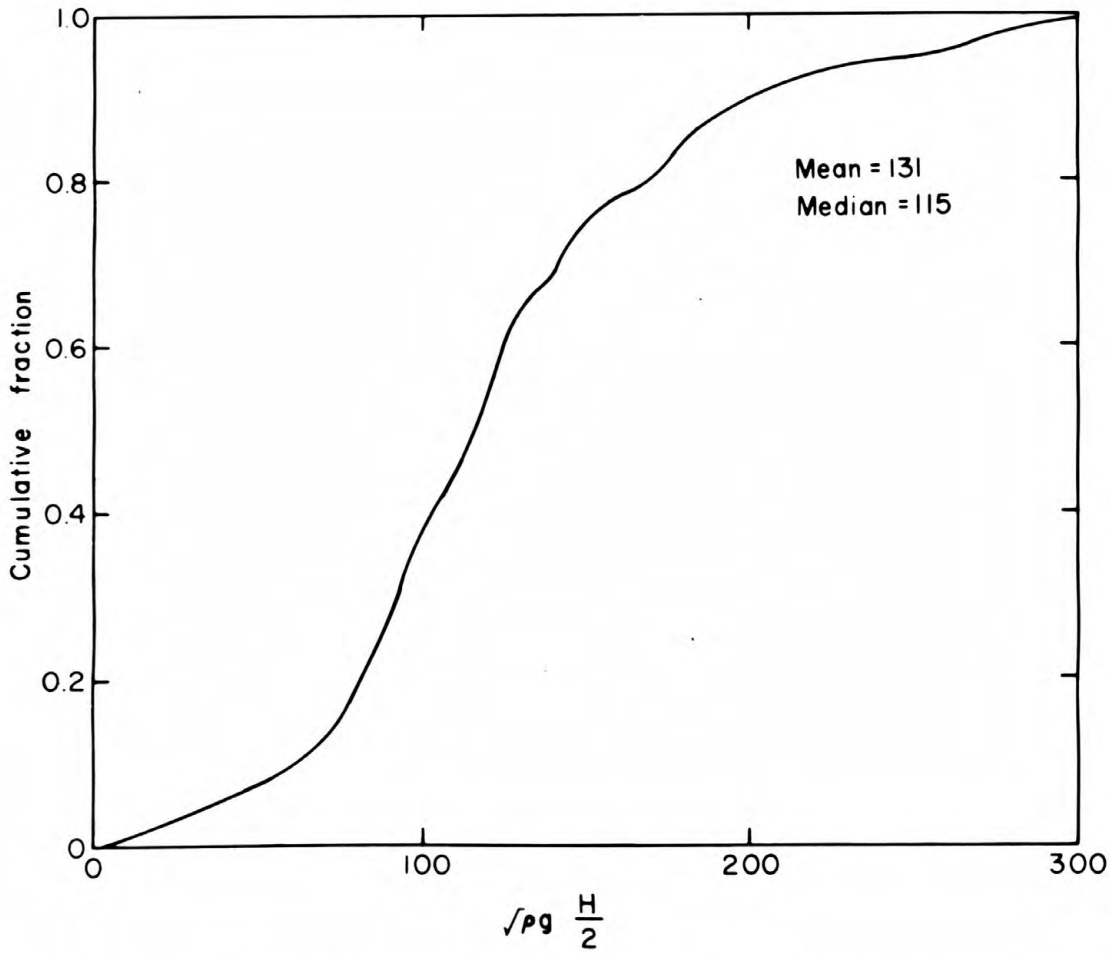

Figure 9.--Cumulative frequency of values of $\sqrt{\rho g}\ H/2$ (equation 12) for lunar data on secondary impact craters using an ejection angle of 45°.

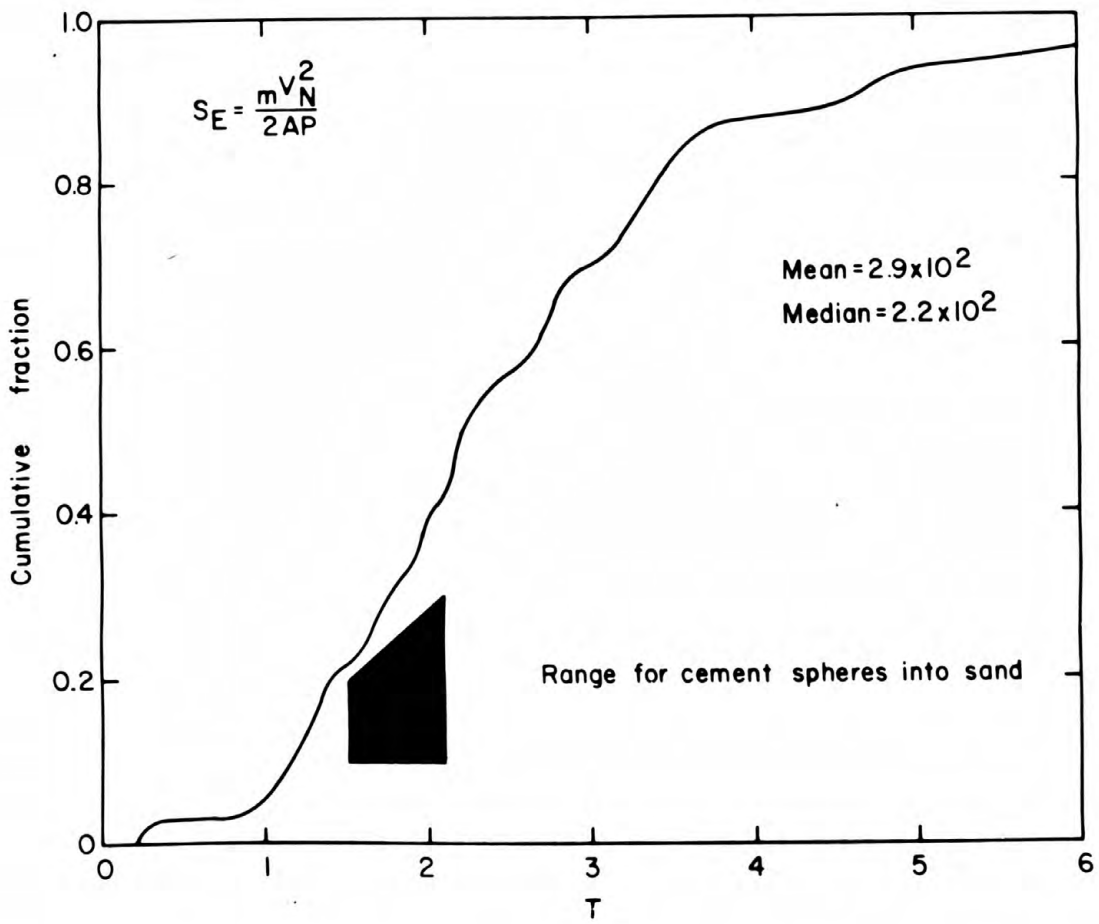

Figure 10.--Cumulative frequency of values of T (equation 13) for lunar data for secondary impact craters. Range of experimental values of T for cement spheres into fine sand are included. Assumed ejection angle for lunar data is 45°.

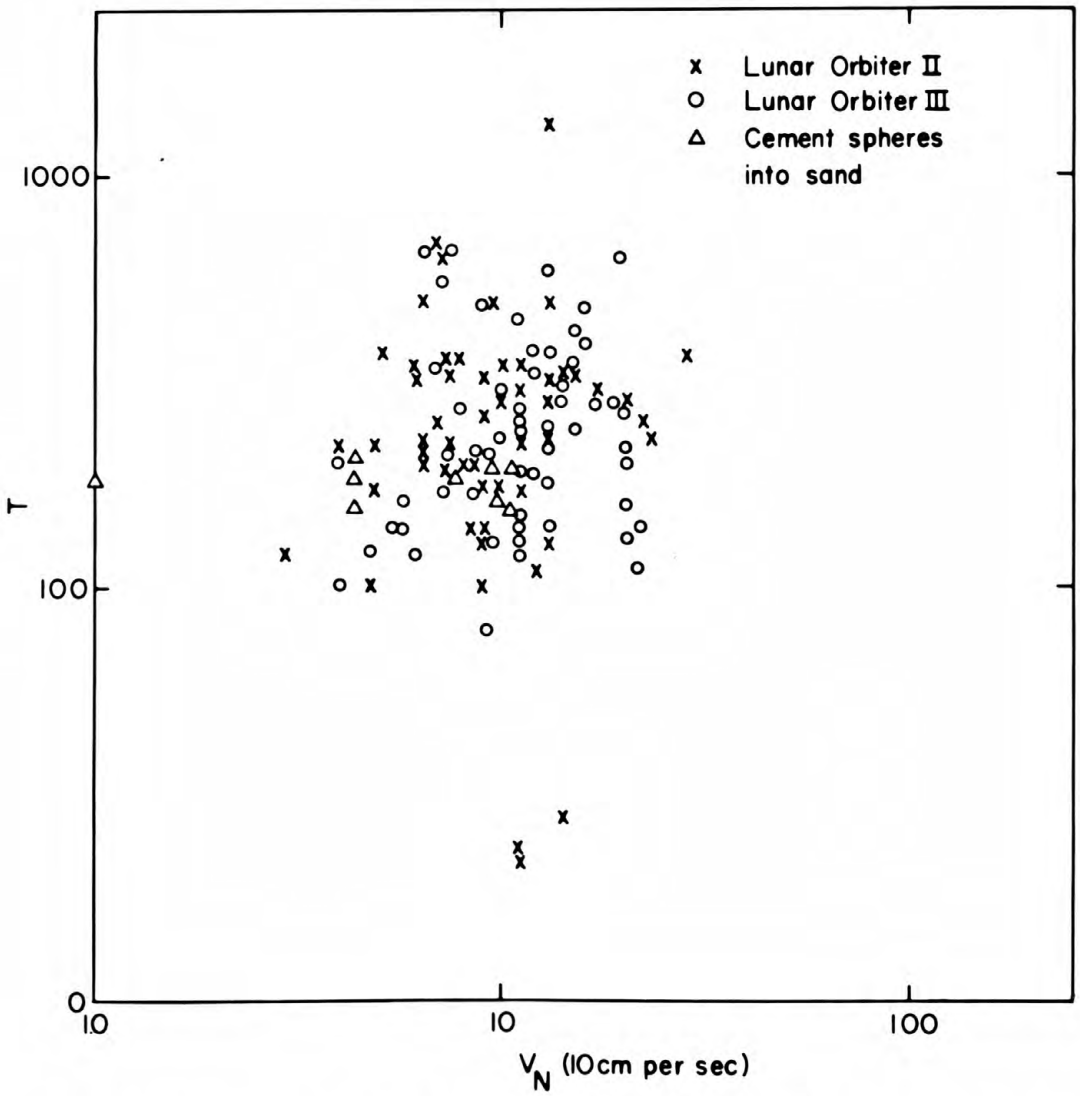

Figure 11.--Comparison of lunar data values of the coefficient T for secondary impact craters (equation 13) and data on cement spheres. An ejection angle of 45° is used for the lunar data.

the static bearing capacities whereas they should be larger, (2) the constants computed using equations 8, 10, 11, and 12 are too low, and (3) Surveyor program and Apollo 11 results suggest that a larger value of cohesion, soil, density, and block density should be used in equation 6. Tables 6 and 7 show the mean values for the lunar data corrected for an ejection angle of 60° and 70° along with suitable adjustments for the change in acceleration of gravity at the lunar surface. Comparison of the constants for the Mortensen equation, the Clark and McCarty equation, and the Moore equation indicated ejection angles near 60° to 70° are more reasonable than 45°. In addition, the use of a large value for cohesion and soil density would be permitted in the Nara equation. Additionally, the Mortensen and the Clark and McCarty equations become compatible for ejection angles of 60° to 70°.

Determination of bearing capacities and penetration resistance using boulder tracks and secondary impact craters are at best order of magnitude estimates because of a number of problems inherent in the technique and available data. The calculations using the static analysis of boulder tracks require knowledge of any six of the following seven properties: (1) the block density, (2) soil density, (3) cohesion, (4) angle of internal friction, (5) local slope, (6) contact area between the boulder and the surface, and (7) the boulder dimensions. The seventh property and the bearing capacity can then be calculated. Reasonable numbers for the densities and cohesions can be obtained from Surveyor and Apollo data but this requires the assumption that some properties are uniform. This assumption may be incorrect. Local slopes are difficult to obtain because boulder tracks are normally found on steep slopes where photoclinometric results are the least reliable. Some estimates can be obtained using photogrammetric techniques combined with the assumption that slopes are uniform between two widely separated points. The contact area between the boulder and the surface is virtually impossible to measure using vertical photographs because the boulder conceals

Table 6.--Computed mean values and coefficients in equations 3, 4, 8, 10, and 12 using an ejection angle of 60° and gravitational adjustment

Equation number	Letter designation	Increase in mean for 60° ejection angle	New calculated mean for 60° ejection angle	Gravity adjustments		Terrestrial value
				Johnson and others (1969) (1.4) or $(1.4)^3$	Chabai (1965) (1.56) or $(1.56)^3$	
3	S_E	1.74X	43.8×10^5 dynes per cm^2	61.3×10^5	68.3×10^5	
4	$2S_c$	1.32X	25.3×10^5 dynes per cm^2	69.4×10^5	96.1×10^5	
8	M	1.32X	23.0	63.0	87.3	86.4
10	J/2	1.2X	16.1	22.5	25.1	27.6
12	$\sqrt{\rho g}$ H/2	1.32X	173	242	270	646-725

Table 7.--Computed mean values and coefficients in equations 3, 4, 8, 10, and 12 using an ejection angle of 70° and gravitational adjustments.

Equation number	Letter designation	Increase in mean for 70° ejection angle	New calculated mean for 70° ejection angle	Gravity adjustments: Johnson and others (1969) (1.4) or $(1.4)^3$	Gravity adjustments: Chabai (1965) (1.56) or $(1.56)^3$	Terrestrial value
3	S_E	2.92X	73.6×10^5 dynes per cm^2	103×10^5	161×10^5	
4	$2S_c$	1.87X	35.9×10^5 dynes per cm^2	98.5×10^5	136×10^5	
8	M	1.87X	32.5	89.2	123	86.4
10	J/2	1.43X	19.2	27.2	30	27.6
12	$\sqrt{\rho g}$ H/2	1.71X	224	314	349 504 (see Moore 1967b)	646-725

the bearing area. The height and shape of the boulder are difficult to measure because many boulders are not much larger than the photographic resolution of the Orbiter photographs and local slopes affect estimates of boulder height using shadow techniques. Indeed, measurements of dimensions of boulders at the end of tracks in Montana using vertical photographs differ significantly from those measured on the ground and the corresponding estimates of contact areas are not the same. Additional uncertainties are inherent in the use of secondary impact craters to estimate bearing capacities: (1) ejection angles are unknown and data on experimental impact cratering show a wide range of ejection angles for various materials and at various times during crater growth, (2) measured ejection distances of the blocks from their point of origin in the primary crater are approximate, (3) interpretations of associations of blocks and craters are sometimes ambiguous, (4) the orientation of the blocks at impact, which are normally triaxial, are unknown, (5) shape factors are often ambiguous because of restricted photographic resolution, (6) data and theories on low velocity impact are not in perfect agreement, and (7) kinetic energies of rotation of the blocks at impact, which are unknown and uncalculable, could easily exceed the kinetic energy of translation and thus might appreciably affect the crater size.

Conclusions

1. The bearing capacities of the lunar surface materials obtained using boulders at the end of tracks shown on Lunar Orbiter II and III photographs are consistent with a soil-like material or regolith that is easily deformed. Computed friction angles which average 17° are lower than those obtained by Surveyor spacecraft.
2. The average dynamic penetration resistance computed for

secondary impact craters with the Euler and modified Charter's-Summer's equations are consistent with an easily deformed soil-like material or regolith at the lunar surface. The dynamic penetration resistances for each block for assumed ejection and impact angles of 45° are generally comparable to static bearing capacities computed for each block when the friction angles are between about 30° and 40°.

3. The scatter in the lunar data on secondary impact craters using the low velocity impact equations of Clark-McCarty, Mortensen, and Moore is less than that for the Euler and modified Charter's-Summer's equations. Constants calculated for the lunar data using the Clark-McCarty, Mortensen, and Moore equations are substantially less than those obtained for sand on earth when the ejection and impact angles are taken as 45°. Better agreement between lunar and terrestrial constants are obtained when ejection angles are increased to 60-70° and the effect of the low acceleration of gravity is taken into account. Additionally, average constants for the Clark-McCarty and Mortensen equations become consistent with each other for these larger ejection-impact angles.
4. Uncertainties in the assumptions and measurements used to estimate static bearing capacities with boulders at the end of tracks and penetration resistances using secondary impact craters make such estimates, at best, approximate. They do indicate that the lunar surface materials are soil-like and easily deformed and that the lunar surfaces have sufficient strenght to support the blocks.

REFERENCES

Boeing Company, 1967a, Lunar Orbiter II-postmission photo supporting data: prepared for Natl. Aeronautics and Space Adm. under contract NAS 1-3800, NASA-CR-66478, 529 p.

_____ 1967b, Lunar Orbiter III-postmission photo supporting data: prepared for the Natl. Aeronautics and Space Adm. under contract NAS-1-3800, NASA-CR-66469, 503 p.

Bryan, G. M., 1962, Oblique impact of high velocity steel pellets on lead targets: Hypervelocity Impact, 5th Symposium, Denver (Oct. 30-Nov. 1, 1961), Proc., v. 1, pt. 2, p. 511-534.

Chabai, A. J., 1965, On scaling dimensions of craters produced by buried explosives, Jour. Geophys. Research, v. 70, no. 20, p. 5075-5098.

Charters, A. C., and Summers, J. L., 1959, Some comments on the phenomena of high-speed impact: Silver Spring, Maryland, Decennial Symposium, May 26, 1959, White Oak U.S. Naval Ordnance Laboratory, 21 p.

Choate, Raoul, 1966, Lunar slope angles and surface roughness from Ranger photographs: Jet Propulsion Lab. Tech. Rept. 32-994, p. 411-432.

Choate, Raoul, Batterson, S. A., Christensen, E. M., Hutton, R. E., Jaffe, L. D., Jones, R. H., Ko, H. Y., Spencer, R. L., and Sperling, F. B., 1968, Lunar surface mechanical properties, in Surveyor VII, A preliminary report: Natl. Aeronautics and Space Adm., NASA-SP-173, p. 87-119.

Choate, Raoul, Batterson, S. A., Christensen, E. M., Hutton, R. E., Jaffe, L. D., Jones, R. H., Ko, H. Y., Scott, R. F., Spencer, R. L., Sperling, F. B., and Sutton, G. H., 1969, Lunar surface mechanical properties, in Surveyor program results: NASA-SP-184, p. 129-169.

Christensen, E. M., Batterson, S. A., Benson, H. E., Chandler, C. E., Jones, R. H., Scott, R. F., Shipley, E. N., Sperling,

F. B., Sutton, G. H., 1967a, Lunar surface mechanical properties--Surveyor I: Jour. Geophys. Research, v. 72, no. 2, p. 801-813.

Christensen, E. M., Batterson, S. A., Benson, H. E., Choate, Raoul, Jaffe, L. D., Jones, R. H., Ko, H. Y., Spencer, R. L., Sperling, F. B., Sutton, G. H., 1967b, Lunar surface mechanical properties, in Surveyor III, A preliminary report, Natl. Aeronautics and Space Adm., NASA-SP-146, p. 94-120.

Christensen, E. M., Batterson, S. A., Benson, H. E., Choate, Raoul, Jaffe, L. D., Jones, R. H., Ko, H. Y., Spencer, R. L., Sperling, F. B., and Sutton, G. H., 1968a, Lunar surface mechanical properties at the landing site of Surveyor III: Jour. Geophys. Research, v. 73, no. 12, p. 4081-4094.

Christensen, E. M., Batterson, S. A., Choate, Raoul, Hutton, R. E., Jaffe, L. D., Jones, R. H., Ko, H. Y., Schmidt, F. N., Scott, R. F., Spencer, R. L., and Sutton, G. H., 1968b, Lunar surface mechanical properties: Jour. Geophys. Research, v. 73, no. 22, p. 7169-7192.

Christensen, E. M., Batterson, S. A., Benson, H. E., Choate, Raoul, Hutton, R. E., Jaffe, L. D., Jones, R. H., Ko, H. Y., Schmidt, F. N., Scott, R. F., Spencer, R. L., Sperling, F. B., and Sutton, G. H., 1968c, Lunar surface mechanical properties, in Surveyor VI, A preliminary report: Natl. Aeronautics and Space Adm., NASA-SP-166, p. 41-95.

Clark, L. V., and McCarty, J. L., 1963, The effect of vacuum on the penetration characteristics of projectiles into fine particles: Natl. Aeronautics and Space Adm. Tech. Note, NASA TN-D-1519, 26 p.

Cook, M. A., and Mortensen, K. S., 1967, Impact cratering in granular materials: Jour. Appl. Physics, v. 38, no. 13, p. 5125-5128.

Eggleston, J. M., Patterson, A. W., Throop, J. E., Arant, W. H., and Spooner, D. L., 1968, Lunar "Rolling Stones": Photogrammetric Eng. v. 34, p. 246-255.

Felice, A. L., 1967, Lunar surface strength estimate from Orbiter II photograph: Science, v. 156, no. 3781, p. 1486-1487.

Gault, D. E., Quaide, W. L., Oberbeck, V. R., 1965, Interpreting Ranger photographs from impact crater studies, in Hess, W., Menzel, D. H., and O'Keefe, J. A., eds., The nature of the lunar surface: Baltimore, Md., The Johns Hopkins Press, p. 125-154.

Goldsmith, Werner, 1960, Impact, the theory and physical behavior of colliding solids: London, Edward Arnold Ltd., 379 p.

Grolier, M. J., Moore, H. J., and Martin, G. L., 1968, Lunar block tracks, in A preliminary geologic evaluation of areas photographed by Lunar Orbiter V including an Apollo landing analysis of one of the areas: Langley Research Center, Langley Station, Hampton, Va., Langley Working Paper LWP 506, app. A, p. 143-154.

Hanks, B. R., and McCarty, J. L., 1966, Investigation of the use of penetrometers to determine the capability of dust materials to support bearing loads: Natl. Aeronautics and Space Adm. Tech. Note NASA TN-D-3200, 89 p.

Hovland, H. J., and Mitchell, J. K., 1969, Friction angle of lunar surface soils estimated from boulder tracks: Space Sciences Laboratory, Lunar Surface Engineering Properties Experiment Definition, Second Quarterly Report, Univ. of California, 117 p.

Jaffe, L. D., 1965, Strength of the lunar dust: Jour. Geophys. Research, v. 70, no. 24, p. 6139-6146.

_____1967, Surface structure and mechanical properties of the lunar maria: Jour. Geophys. Research, v. 72, no. 6, p. 1727-1731.

Johnson, S. W., Smith, J. A., Franklin, E. G., Moraski, L. K., and Teal, D. J., 1969, Gravity and atmospheric pressure

effects on crater formation in sands: Jour. Geophys. Research, v. 74, no. 20, p. 4838-4850.

Karafiath, L. L., and Nowatzki, E. A., 1968, Surveyor V landing: the effect of slope on bearing capacity: Science, v. 161, no. 3841, p. 601-603.

Kuiper, G. P., Strom, R. G., and LePoole, R. S., 1966, Interpretation of the Ranger records, in Ranger VIII and IX, pt. II, Experimenters' analyses and interpretations, Jet Propulsion Lab. Tech. Rept. no. 32-800, p. 35-248.

Mitchell, J. K., Quigley, D. W., Smith, S. S., 1969, Impact records as a source of lunar surface material property data, in Materials studies related to lunar surface exploration, chap. 4: Space Sciences Laboratory, Univ. of California, Berkeley, Calif., 41 p.

Moore, H. J., 1967a, Nature of lunar surface materials as indicated by craters on Lunar Orbiter I and II, in Preliminary geologic evaluation and Apollo landing analysis of areas photographed by Lunar Orbiter II: Langley Research Center, Langley Station, Hampton, Va., Langley Working Paper LWP 363, app. A, p. 106-110.

_____, 1967b, The use of ejected blocks and secondary impact craters as penetrometers on the lunar surface, in Preliminary geologic evaluation and Apollo landing analysis of areas photographed by Lunar Orbiter III: Langley Research Center, Langley Station, Hampton, Va., Langley Working Paper LWP 407, app. A, p. 108-121.

Moore, H. J., and Lawry, M., 1968, Secondary Impact Craters, in A preliminary geologic evaluation of areas photographed by Lunar Orbiter V including an Apollo landing analysis of one of the areas: Langley Research Center, Langley Station, Hampton, Va., Langley Working Paper LWP 506, app. B, p. 155-157.

Mortensen, K. S., 1967, A fundamental study of cratering in granular materials with an application to lunar craters [Thesis,

Ph.D., University of Utah, Salt Lake City, Utah]: Ann Arbor, Mich., University Microfilms, 132 p.

Myerhof, G. G., 1951, The ultimate bearing capacity of foundations: Géotechnique, v. 2, no. 4, p. 301-332.

Nara, H. R., and Denington, R. J., 1954, Ricochet and penetration of steel spheres in clay and sand soils: Cleveland, Ohio, Project Doan Brook Tech. Memo E-7, Case Institute of Technology, Cleveland, Ohio, AD-59883, 61 p.

O'Keefe, J. A., and Scott, R. F., 1967, Chondritic meteorites and the lunar surface: Science, v. 158, no. 3805, p. 1174-1176.

Partridge, W. S. and Van Fleet, H. B., 1958, Similarities between lunar and high-velocity impact craters: Astrophys. Jour., v. 127, p. 416-419.

Pyrz, A. P., 1969, Gravity effects on low velocity penetration of a projectile into a cohesionless medium: Air Force Inst. of Technology, Air University USAF, School of Engineering, Wright-Patterson Air Force Base, Ohio, 135 p.

Scott, R. F., 1963, Principles of soil mechanics: Reading, Mass. Addison-Wesley, 550 p.

Scott, R. F., and Jaffe, L. D., 1966, Lunar surface strength: Implications of Luna 9 landing: Science, v. 153, no. 3734, p. 407-408.

Scott, R. F. and Roberson, F. I., 1968a, Surveyor III--Soil mechanics surface samples: Lunar surface tests, results, and analysis: Jour. Geophys. Research, v. 73, no. 12, p. 4045-4080.

_____ 1968b, Soil mechanics surface sampler, in Surveyor VII, A preliminary report, Natl. Aeronautics and Space Adm. Spec. Pub. NASA SP-173, p. 121-161.

_____ 1969, Soil mechanics surface sampler, in Surveyor program results: Natl. Aeronautics and Space Adm. Spec. Pub. NASA SP-184 p. 171-179.

Scott, R. F., Roberson, F. I., and Clary, M. C., 1967, Soil mechanics surface sampler: Lunar surface tests and results, in Surveyor III, A preliminary report, Natl. Aeronautics and Space Adm. Spec. Pub. NASA SP-146, p. 61-93.

Shoemaker, E. M., Batson, R. M., Holt, H. E., Morris, E. C., Rennilson, J. J., and Whitaker, E. A., 1967, Television observations from Surveyor V, in Surveyor V, A preliminary report, Natl. Aeronautics and Space Adm. Spec. Pub. NASA-SP-163, p. 9-42.

Terzaghi, Karl, 1948, Theoretical soil mechanics: New York, John Wiley and Sons, Inc., 509 p.

Young, C. W., 1967, The development of empirical equations for predicting depth of an earth-penetrating projectile: Sandia Corp. Development Report SC-DR-67-60, 41 p.